

## Complex plasmas: a laboratory for strong correlations

This article has been downloaded from IOPscience. Please scroll down to see the full text article.

2010 Rep. Prog. Phys. 73 066501

(<http://iopscience.iop.org/0034-4885/73/6/066501>)

View [the table of contents for this issue](#), or go to the [journal homepage](#) for more

Download details:

IP Address: 134.245.67.147

The article was downloaded on 20/05/2010 at 07:24

Please note that [terms and conditions apply](#).

# Complex plasmas: a laboratory for strong correlations

M Bonitz<sup>1</sup>, C Henning<sup>1</sup> and D Block<sup>2</sup>

<sup>1</sup> Institut für Theoretische Physik und Astrophysik, Christian-Albrechts-Universität zu Kiel, D-24098 Kiel, Germany

<sup>2</sup> Institut für Experimentelle und Angewandte Physik, Christian-Albrechts-Universität zu Kiel, D-24098 Kiel, Germany

E-mail: [bonitz@physik.uni-kiel.de](mailto:bonitz@physik.uni-kiel.de)

Received 28 October 2009

Published 20 May 2010

Online at [stacks.iop.org/RoPP/73/066501](http://stacks.iop.org/RoPP/73/066501)

## Abstract

Strong correlations—cooperative behavior due to many-particle interactions—are omnipresent in nature. They occur in electrolytic solutions, dense plasmas, ultracold ions and atomic gases in traps, complex (dusty) plasmas, electrons and excitons in quantum dots and the quark–gluon plasma. Correlation effects include the emergence of long-range order, of liquid-like or crystalline structures and collective dynamic properties (collective modes). The observation and experimental analysis of strong correlations are often difficult, requiring, in many cases, extreme conditions such as very low temperatures or high densities. An exception is complex plasmas where strong coupling can be easily achieved, even at room temperature. These systems feature the strongest correlations reported so far and experiments allow for an unprecedented precision and full single-particle resolution of the stationary and time-dependent many-particle behavior.

The governing role of the interactions in strongly correlated systems gives rise to many universal properties observed in all of them. This makes the analysis of one particular system interesting for many others. This motivates the goal of this paper which is to give an overview on recent experimental and theoretical results in complex plasmas including liquid-like behavior, crystal formation, structural and dynamic properties. It is expected that many of these effects will be of interest also to researchers in other fields where strong correlations play a prominent role.

(Some figures in this article are in colour only in the electronic version)

This article was invited by Gordon Baym.

## Contents

<b>1. Introduction</b>	<b>2</b>	<b>3. Finite systems</b>	<b>8</b>
1.1. Significance of strong correlations in nature	2	<b>4. Structure of plasma crystals</b>	9
1.2. Correlations in charged particle systems	4	4.1. Theoretical models	9
1.3. How to reach the crystal state	4	4.2. Pair distribution function of a strongly coupled plasma	11
<b>2. Physics of complex (dusty) plasmas</b>	<b>5</b>	4.3. Spherically confined crystals: Yukawa balls	11
2.1. Parameter regime	5	4.4. Radial density profile of Yukawa balls	15
2.2. Charging of dust particles	5	<b>5. Dynamical properties</b>	16
2.3. Dust plasma interaction	6	5.1. Normal modes of finite systems	16
2.4. Neutral gas effects	6	5.2. Normal modes of crystals in a spherical harmonic trap	17
2.5. Forces on dust particles	7		
2.6. Dust confinement	7		
2.7. Dust dynamics	7		

5.3. Breathing mode versus monopole oscillation	17	<b>7. Liquid behavior</b>	21
5.4. Normal modes in dusty plasma experiments	18	7.1. Anomalous diffusion	22
5.5. Normal modes of strongly correlated quantum systems	18	7.2. Theoretical description of strong correlations in the fluid state	22
<b>6. Thermodynamics and phase transitions</b>	19	<b>8. Conclusions</b>	24
6.1. Melting in finite systems	20	<b>Acknowledgments</b>	24
6.2. Melting of Yukawa balls: experiment and simulation	21	<b>References</b>	24

## 1. Introduction

This paper is devoted to recent developments in complex (dusty) plasmas—concerned with the realization of strongly correlated behavior of mesoscopic or macroscopic particle ensembles. We will use the term ‘correlated behavior’ as a synonym for deviations from the trivial ideal gas behavior. The origin of correlations is the interactions between the particles missing (by definition) in an ideal gas, and a typical Hamiltonian has the form

$$H = \sum_{i=1}^N \frac{p_i^2}{2m} + \sum_{i=1}^N U(\mathbf{r}_i) + \frac{1}{2} \sum_{i \neq j}^N V(|\mathbf{r}_i - \mathbf{r}_j|), \quad (1)$$

where  $U$  is a general external potential and we restrict ourselves to systems with distance-dependent pair interactions.

Correlations have a profound effect on the arrangement of the particles in momentum and coordinate space. While in an ideal gas ( $V \equiv 0$ ) in thermodynamic equilibrium the momentum distribution is given by a Maxwellian (Fermi or Bose function, in the quantum case), the momentum distribution of a non-ideal quantum system may be substantially different leading to enhanced population of high-momentum states and long tails, see e.g. [1] and references therein. In contrast, in a classical system the momentum distribution is always Maxwellian. However, both in classical and quantum systems, much more striking is the effect of correlations on the spatial arrangement of particles. While in an ideal gas the particle positions are independent (the probability  $g(r)$  to find two particles at a distance  $r$  is independent of  $r$ ), in a correlated system the pair distribution  $g(r)$  exhibits strong modulations. This is caused by strong interactions<sup>3</sup> which favor certain distances of neighboring particles (attractive potential) or suppress close encounters (repulsive potential). This non-trivial spatial arrangement of particles will be in the focus of this review. We will entirely concentrate on classical systems since, so far, in dusty plasma experiments quantum effects are not accessible. Nevertheless, the observed strong correlation phenomena are expected to be of—at least qualitative—relevance also for quantum systems.

The strength of correlations is conveniently measured by the coupling parameter,  $\Gamma = \langle |V| \rangle / \langle K \rangle$ , the ratio of the mean interaction energy to the kinetic energy  $K$ , see equation (2). Using the parameter  $\Gamma$ , the *universal trends* in all correlated systems can be highlighted and quantified: ideal gas-like behavior occurs for  $\Gamma \ll 1$ , liquid-like short-range

order for  $\Gamma \gtrsim 1$  and crystalline long-range order for  $\Gamma \gtrsim 100$ . While the precise values are different for classical and quantum systems and depend on the system dimensionality, the form of the interaction potential and the external potential  $U$ , many correlation phenomena are observed in all many-particle systems, independent of their specific nature. This makes the analysis of correlation effects in one system very interesting also for other fields of physics. This is particularly true also for complex plasmas. These systems not only allow one to produce the strongest correlations known today ( $\Gamma$  values exceeding 1.000 have been realized), but they also allow for an unprecedented accuracy of analysis. As we will show in this review, many quantities such as crystal structure, pair distribution function, normal modes and even single-particle trajectories can be directly observed in the experiment with full time resolution, making this field an ideal test case for theoretical concepts, with high predictive capability also for other fields.

### 1.1. Significance of strong correlations in nature

Let us start with a brief overview on correlation effects in various fields of physics. Historically, the first encounter of strong non-ideality effects was, probably, the *gas–liquid phase transition*. Condensation effects clearly showed a deviation from ideal gas behavior and the breakdown of the ideal equation of state  $p = nk_B T$ . The phenomenological solution of this problem was achieved by the introduction of a modified equation of state, such as the van der Waals equation, which incorporates interactions between the molecules. Despite its model character it correctly captures the non-perturbative nature of the phase transition—a manifestation of strong correlations with  $\Gamma \gtrsim 1$ .

Modern statistical mechanics have put the theoretical analysis of correlations on a firm ground. Here, pioneering work started in the description of fluids, in particular, in *electrolytic solutions*. Charged molecules in a solvent (such as water) interact via strong Coulomb forces and may exhibit strong correlations, see e.g. [2, 3]. The consequences are strong static and dynamical screening effects first described by Debye and Hückel [4]. Also, the formation of chemical bound states of positive and negative ions, described by Planck [5], Arrhenius [6], Bjerrum [7], and others strongly influences the thermodynamic and transport properties [2]. The modern statistical treatment of non-ideal fluids is based on a rigorous derivation from mechanics which leads to the hierarchy for the reduced distribution functions of Bogolyubov [8] and others (BBGKY hierarchy, see e.g. [1]). The proper treatment of

<sup>3</sup> Spatial modulations of particles may also be caused by spin statistics, but this will not be considered here.

strong correlations in classical fluids is achieved with self-consistent closure approximations such as the Percus–Yevick (PY) and hypernetted-chain (HNC) approximation, e.g. [3], which will be discussed in section 7.2.

Screening and, in particular, neutral bound state formation strongly limit the interaction energy and coupling strength in electrolytes. This limitation is overcome in *colloidal dispersions* (‘complex fluids’) where mesoscopic particles with a size in the range 1 nm to 10  $\mu\text{m}$  are embedded into a fluid solvent. These particles can become highly charged and strongly interacting—the same mechanism which forms the basis of strongly coupled complex plasmas, see section 2. Strong Coulomb interaction together with dense packing of particles gives rise to strong spatial correlations leading to the formation of gels, crystals and glass states. These systems differ from dusty plasmas by the existence of a liquid solvent causing a strong damping of the particle motion. For recent overviews, see [9, 10] and references therein.

Correlations also play a significant role in the description of the *electronic properties of solids*. The physical properties of many materials such as simple metals, semiconductors and insulators are characterized by moderate coupling and are, thus, successfully explained by modern solid-state physics within a quasi-particle description. There exist, however, numerous materials such as transition metals and their oxides, in which electrons experience strong Coulomb interactions because of their spatial confinement into narrow bands, see e.g. [11]. In these systems, a mean-field description—as in usual band theory—fails<sup>4</sup>, (e.g. [12]), and correlations play a crucial role. Such materials are often extremely sensitive to external parameters (fields) which can lead to huge changes in the resistivity at the metal–insulator transition [13–15], to volume-collapse transitions of rare earth metals [16], to high transition temperatures of cuprate superconductors, gigantic thermoelectric power [17] or colossal magnetoresistance [18]. Successful theoretical approaches to strongly correlated electrons include model Hamiltonians such as the Hubbard model [12] or dynamical mean-field theory [19].

Another field where strong correlations are becoming increasingly important is *ultracold fermionic or bosonic atoms* confined in traps or in the periodic potential of an optical lattice [20]. The full control over all relevant parameters in these systems provides a novel approach for the study of correlation effects on a quantitative level. Exciting correlation effects include the quantum phase transition from a superfluid to a Mott-insulating phase [21], even in the standard regime where the average interparticle spacing is much larger than the scattering length. Thus, these extremely dilute gases can no longer be described by a mean-field picture of non-interacting quasi-particles, but require inclusion of strong correlations. In addition to the optical lattices, the exploration of strong correlations with ultracold gases is possible by using Feshbach resonances [22]. The possibility of tuning the interaction strength allows, e.g., for the exploration of the crossover, which takes place in two-component fermionic systems, from a molecular Bose–Einstein condensate of tightly bound pairs

to a BCS superfluid of weakly bound Cooper pairs [23]. This crossover promises insights into recent questions of quantum fluids and high-transition-temperature superconductors [24].

One of the major advantages of ultracold atoms is the possibility of dynamically changing the relevant parameters such as the relative strength of the kinetic and interaction energy, and thus studying the real-time dynamics of strongly correlated systems. However, this requires precise experiments under difficult conditions. In addition to the creation of ultralow temperatures and preparation of adequate traps [25], the detection methods need to be essentially correlation-sensitive (for a recent overview, see [26]). These and future experiments may substantially benefit from the experience in dusty plasmas where the diagnostics of individual particles and of correlation effects have reached a mature state, as we will show in section 3.

While the emergence of correlations at low temperatures may not be that surprising, strongly correlated systems at high temperatures are even more exciting. In complex plasmas Coulomb crystallization is easily reached at room temperature which is one of the reasons for the impressive experimental progress. An extreme and entirely different very recent example of high temperature systems is the *quark–gluon plasma* (QGP). This state of matter consisting of deconfined quarks and gluons plays a major role in the description of the early universe and of ultra-compact matter such as in neutron or quark stars. It is experimentally studied in relativistic heavy-ion collisions at the Relativistic Heavy Ion Collider (RHIC) at Brookhaven National Laboratory [27–30] and at CERN at the Super Proton Synchrotron (SPS) [31, 32] and the Large Hadron Collider (LHC) [33]. While it was originally expected to observe a weakly interacting gas of quarks and gluons [34, 35] the experiments at RHIC give strong evidence that the QGP actually behaves like a strongly coupled fluid with extremely low viscosity [36, 37]. This view is now supported by first-principle QCD lattice calculations [38, 39]. Interestingly, the governing role of correlations may allow for the application of simpler theoretical models and simulations of the QGP, including semiclassical molecular dynamics [40–42] and quantum Monte Carlo simulations [43]. The analogy of the collective properties of the QGP and electromagnetic complex plasmas has been pointed out recently [44, 45] where it was suggested that results from the latter may give qualitative insights into properties of the former.

So far we have discussed various examples (this is by no means a complete list) of different systems where strong correlations occur. It is amazing to see how enormously different these systems are and how strongly their parameters differ. An illustration is given in figure 1 where a density–temperature plane is shown which spans tens of orders of magnitude. Extreme cases in density are complex plasmas, at the low end, and the QGP, at the high density limit; the difference is more than 35 orders of magnitude. Similarly, their difference in temperature is about 10 orders of magnitude; another 6 orders of magnitude lower than complex plasmas are the ultracold atomic gases.

<sup>4</sup> Interaction effects can be divided into mean-field and correlation contributions. This will be discussed in more detail in section 4.4



systems. Ion crystallization in Paul traps was achieved more than two decades ago at milli-kelvin temperatures (e.g. [46]), and is now routinely studied in a number of laboratories, see e.g. [47]. Crystal geometries range from linear strings to spheres and are similar to the structures observed in complex plasmas. The main differences compared with the latter are the existence of a pure Coulomb interaction between the ions and the absence of additional plasma components. Other laboratory systems where strong correlations play a role are dense plasmas produced by intense lasers or ion beams which gave rise to the new field of ‘warm dense matter’ (for a recent overview, see [48, 49]). Finally, we mention the field of ultracold plasmas where a strongly correlated plasma is produced by photoionization of a trapped neutral gas, previously cooled to micro-kelvin temperatures [50]. However, these experiments are very difficult and have so far reached only moderate coupling strengths,  $\Gamma \sim 3\text{--}4$ , although Coulomb crystallization has been predicted if the plasma could be laser cooled [51] (for recent overviews see [52, 53]).

The reason why these very different systems, spanning so broad regions in density and temperature, possess similar structural and collective properties rests on the fact that the mechanisms governing cooperative behavior are quite universal. To this end, consider the characteristic energy scales of a one-component many-particle system: these are the kinetic energy  $K$  of a particle and the mean interaction energy  $V$  of two nearest neighbors. The ratio of their expectation values forms a dimensionless ‘coupling parameter’ (e.g. [54])

$$\Gamma_a = \frac{|\langle V_a \rangle|}{\langle K_a \rangle} \longrightarrow \frac{Q_a^2}{\bar{r}_a k_B T_a}, \quad (2)$$

where the second expression corresponds to charged particles with charge  $Q_a$  and mean interparticle distance  $\bar{r}_a$ . Interestingly, distinct values of  $\Gamma_a$  separate qualitatively different behaviors: from weak coupling (ideal gas-like) at  $\Gamma_a \ll 1$ , over fluid-like ( $\Gamma_a \gtrsim 1$ ) to very strong coupling,  $\Gamma_a \gtrsim 100$ , where crystal formation occurs because particles have insufficient kinetic energy to leave local minima of the total potential. This scenario of crystallization was first predicted by Wigner for the electron gas in metals [55] and has since then been verified in many systems. The precise values of  $\Gamma_a$  at the freezing point have been obtained by computer simulations and have, over the years, converged to values around 175, in 3D, and 137, in 2D, (e.g. [54, 56]). Thus, in the density–temperature plane, cf figures 1 and 2, lines of constant  $\Gamma$  separate different many-particle behaviors and allow one to qualitatively estimate the characteristic properties of the various physical systems. Other quantities characterizing the correlations will be introduced and discussed in section 4.2.

In a multi-component system,  $\Gamma$  may be different for different species (labeled by subscript ‘ $a$ ’) giving rise to interesting coexistences of different phases. Throughout this paper,  $\Gamma$  will be a key parameter for characterizing the strength of correlations. Finally, for completeness, we note that the definition of  $\Gamma_a$  is restricted to classical systems. For quantum systems characterized by a value of the degeneracy parameter  $\chi_a$  ( $\Lambda_a$  denotes the thermal de Broglie wave length),

$$\chi_a = n_a \Lambda_a^3, \quad \Lambda_a^2 = \frac{h^2}{2\pi m_a k_B T_a}, \quad (3)$$

exceeding unity the kinetic energy has to be replaced by its quantum expression. This gives rise to a quantum coupling parameter (Brueckner parameter):

$$r_{sa} = \frac{\bar{r}_a}{a_B}, \quad (4)$$

where  $a_B$  denotes the Bohr radius; for more details and further references on strongly correlated quantum systems see [54].

### 1.3. How to reach the crystal state

With the coupling parameter  $\Gamma$  at hand it is straightforward to discuss different ways toward strong coupling and, ultimately, crystal formation.

- (i) The first approach to increase  $\Gamma$  is to lower the temperature. The main obstacle in a two-component neutral plasma is the recombination of electrons and ions leading to neutral bound states (atoms or molecules) which interact much weaker. How to realize Coulomb crystals in a two-component plasma was recently discussed in [57]. Alternatively, recombination can be entirely avoided by working with a single charge species, i.e. with a non-neutral plasma. This is realized with ions in electrostatic traps which are required to stabilize the charges against Coulomb repulsion. Typical temperatures are in the milli-kelvin range (e.g. [47]); see section 1.2.
- (ii) The second approach consists of increasing the pair interaction by reducing the interparticle distance. This requires a substantial plasma density which exists in certain astrophysical objects or laboratory environments (e.g. laser or ion beam compression); see section 1.2.
- (iii) There exists an alternative to increase the pair interaction at fixed kinetic energy and density which consists of increasing the particle charge. This was first predicted by Ikezi [58] and confirmed by simulations [59]. This is the key idea to form crystals in dusty (complex) plasmas.

What is remarkable about the third approach is that it allows one to choose very ‘friendly’ experimental conditions—room temperature and low density (large interparticle distance) such that individual particles can be directly detected. This is illustrated in figure 1 by the line  $\Gamma = 175$ ,  $Z = 1 \times 10^4$  which is located eight (!) orders of magnitude higher in temperature than the corresponding line  $\Gamma = 175$  for singly charged particles such as those used in ion traps.

The outline of this paper is as follows: we first discuss the main issues of dusty plasma experiments and the question how strong correlations are achieved experimentally in section 2. This is followed by a discussion of the peculiarities of plasma crystals in finite systems containing several tens to several hundreds of dust particles in section 3. These finite systems, in particular spherically symmetric systems, allow for a very clear analysis and comparison of experiments with theory and are, therefore, in the focus of the remaining sections. We discuss in detail the structure of plasma crystals (section 4), their dynamical behavior and collective oscillations (section 5) and their thermodynamic properties and melting behavior (section 6). Finally, we analyze the properties of the liquid state (section 7) and conclude with a brief discussion and outlook.

## 2. Physics of complex (dusty) plasmas

A complex plasma contains electrons, ions and a third comparably large and heavy species, namely dust particles. This combination is found in astrophysical situations [60] as well as technical applications [61]. However, in addition complex plasmas are an ideal tool to study fundamental properties of strongly coupled matter. The discovery that the dust particles in complex plasmas can form crystalline structures [62–64] has opened a new field of research which allows one to obtain a microphysical picture of strongly coupled matter. After 15 years, a broad spectrum of experiments, simulations and theoretical approaches has achieved a considerable understanding of structural and dynamical processes in complex plasmas. A complete survey of the entire field of complex and dusty plasmas is of course beyond the scope of this review and the reader is referred to recent monographs [60, 61, 65–68] and a new review [69]. However, to show that complex plasmas are indeed a laboratory for strong correlations this review will focus on plasma crystals and in particular mesoscopic 3D systems. For this purpose, this section will briefly introduce the basics of complex plasmas to provide the physical background for the following sections and to hint at some peculiar features of complex plasmas which are not found in other systems and which make complex plasmas interesting by themselves.

### 2.1. Parameter regime

Compared with other strongly coupled systems, complex plasmas have several advantages. Firstly, they are stable under laboratory conditions. This means dust particles can be trapped at room temperature and kept in a desired dynamical state for hours which is beneficial for any diagnostic purpose and generally leads to high accuracy of the measurements due to excellent statistical properties. Secondly, these complex plasmas can consist of millions down to just a very few particles, i.e. finite size effects are accessible. Thirdly, typical densities of 1–50 particles/mm<sup>3</sup> and particle diameters of a few micrometers result in a high optical transparency even for macroscopic dust clouds. This transparency can be used to illuminate particles at arbitrary positions, i.e. even at the center of large clouds, and to resolve the scattered light of individual particles with conventional CCD cameras [70, 71] or to manipulate individual particles *in situ* [72]. Fourthly, the charge-to-mass ratio of dust particles is small, and hence the dynamic response is slow. The dust plasma frequency  $\omega_{pd}$  is on the order of several hertz and, therefore, the frame rate of CCD cameras is sufficient to study dynamic processes in great detail. Finally, complex plasmas are usually produced in a gas discharge with neutral gas pressures of 1–100 Pa. This implies that the system is subject to only moderate damping. As a result, many interesting dynamic phenomena, e.g. waves, can be investigated at a kinetic level. In particular for two-dimensional dust systems, the phase space evolution of all particles is experimentally accessible which provides a unique opportunity for a detailed comparison of experiment and theory. The combination of these nice experimental features is certainly the foundation of the success of complex plasma research.

### 2.2. Charging of dust particles

One of the most important parameters in a complex plasma is the particle charge. Except for astrophysical situations [73], the particle charge is determined by the ambient plasma. For an isolated particle in a collisionless plasma the orbital motion limit (OML) model [74] can be used to determine the floating potential  $\phi_{fl}$  at its surface. Since the electrons are much more mobile than the ions the particles generally charge negatively. The balance of electron (right-hand side) and ion currents (left-hand side) to the dust grain then gives

$$1 - \frac{e\phi_{fl}}{kT_i} = \sqrt{\frac{m_i T_e}{m_e T_i}} \frac{n_e}{n_i} \exp\left(\frac{e\phi_{fl}}{kT_e}\right), \quad (5)$$

where  $T_e(T_i)$  is the electron (ion) temperature,  $m_e(m_i)$  the electron (ion) mass and  $n_e(n_i)$  the electron (ion) density. Although this equation can be solved exactly numerically, for typical laboratory plasmas with  $T_e \gg T_i$  and  $n_i = n_e$ , its solution is well approximated with  $\phi_{fl} \approx -2kT_e/e$ .

With the help of a simple capacitance model [75] the particle charge  $Q_d = Z_d e$  can be determined for spherical particles. Recent simulations [76, 77] show that the charge can deviate notably for arbitrarily shaped particles and even for isolating and conducting particles. However, with the above-mentioned approximation it is possible to find a simple rule of thumb to estimate the particle charge to

$$Z_d \approx 1400 a T_e, \quad (6)$$

where the particle radius  $a$  is given in micrometers and the electron temperature in eV. From this approximation it is obvious that particle charges of the order of  $10^4$  elementary charges are typical for dusty plasmas.

Unfortunately, the validity of the OML model is questionable for many discharge conditions, and different additional processes have to be taken into account, e.g. streaming ions [78–81], collisions [82–84] and dense packing of dust particles [85, 86]. Nevertheless, measurements of the dust charge have been performed by means of resonance methods [63, 87], wave phenomena [88–91] and particle collisions [92], and they confirm that the OML model can be used to estimate an upper limit for the particle charge. Ivlev *et al* have shown that in a supersonic flow the charge distributions become inhomogeneous and substantially deviate from the OML model [93]. A completely different approach to calculate the particle charge has been proposed recently by Bronold *et al* [94]. Their physisorption-inspired model for the formation of surface charges allows one to describe the charging and shielding of dust grains and is an interesting alternative to the existing models.

Finally, it is important to mention that the particle charge in a dusty plasma is in general variable. Firstly, the floating potential depends on the plasma parameters, and these usually have a space dependence. Secondly, at high dust densities the plasma losses on the particles reduce the electron and ion densities [95–97] and, in addition, the quasi-neutrality condition and the high negative charge of dust grains can give rise to an additional depletion of free electrons [98]. Thirdly,

the particle charge in the sheath of an rf-discharge is slightly modulated due to the modulation of the electron density in the sheath [99]. Fourthly, for small particles with just a few elementary charges the discreteness of the charge of electrons and ions and the stochastic nature of the charging process can create notable charge fluctuations which can even result in short periods where the particles are charged positively [100]. In general, the magnitude of the fluctuations is of the order of  $0.5\sqrt{N}$  [100] and thus, under many experimental conditions, particular those discussed in section 3, charge fluctuations are negligible.

### 2.3. Dust plasma interaction

As pointed out in the previous section, dust grains are charged by the plasma, but at the same time they do affect the plasma. Firstly, plasmas are known to be quasi-neutral. Thus, if a notable amount of negative charge is bounded to the dust, the number of free electrons has to decrease to maintain neutrality. Secondly, the average plasma density will decrease since the continuous recombination of electrons and ions on the dust particle surface is an additional plasma loss. Thirdly, any charged object in a plasma is shielded, and this is certainly the most important fact. Thus, in the direct vicinity of a negatively charged dust particle the ion density will increase and the electron density will decrease. As a result two neighboring dust particles will not interact via their unscreened Coulomb potential. Their interaction is weakened by an additional exponential factor and reads as

$$V(r; \kappa) = \frac{Q^2}{r} e^{-\kappa r}, \quad \kappa^2 = \lambda_D^{-2} = \sum_{a=e,i} \frac{4\pi n_a e_a^2}{k_B T_a}, \quad (7)$$

where the screening parameter  $\kappa$  (inverse screening length  $\lambda_D$ ) is determined by the density  $n_a$  and temperature  $T_a$  of electrons and ions. This type of potential is well known in plasmas and nuclear matter as Debye–Hückel or Yukawa potential, respectively, and is a good approximation for all cases without streaming electrons or ions. However, as soon as ion streaming occurs, the Yukawa potential is shown to be valid only in the direction perpendicular to the ion drift [101], and even there, at large distances, deviations from a Yukawa form have been found [102]. In particular at the plasma boundary, where the ions are supersonic, it was shown by experiments that an ion focus establishes in the wake of a particle. This positive space charge adds an attractive component to the interaction potential and, due to the supersonic character, the resulting particle interaction was shown to be non-reciprocal (e.g. [103, 104]). As a result the particles arrange in chains in the direction of the ion flow (see figure 3(a)). This ion focusing and effective dust–dust attraction were studied in detail experimentally (e.g. [105, 106]), as well as theoretically and with simulations (e.g. [107–112]).

### 2.4. Neutral gas effects

So far the discussion concentrated on the dust particles embedded in a plasma. However, in a typical gas discharge the ionization degree is at maximum of the order of a few

**Table 1.** Summary of important forces acting on dust particles in a plasma environment.

Name	Formulae
Gravitational force	$\mathbf{F}_g = \frac{4}{3}\pi a^3 \rho_d \mathbf{g}$
Electrostatic force	$\mathbf{F}_E = 4\pi \epsilon_0 a \phi_n \mathbf{E}$
Radiation pressure	$\mathbf{F}_r = \gamma \frac{\pi a^2 I_0}{c} \mathbf{R}$
Neutral drag force	$\mathbf{F}_n = -\delta \frac{4}{3}\pi a^2 m_n n_n v_{th,n} (\mathbf{v}_d - \mathbf{v}_n)$
Thermophoretic force	$\mathbf{F}_{th} = -\frac{16}{15} \sqrt{\pi} \frac{a^2 k_n}{v_{th,n}} \nabla T_n$
Ion drag force	$\mathbf{F}_{ion} = \mathbf{F}_{coll} + \mathbf{F}_{orb}$
(after Barnes)	$\mathbf{F}_{coll} = \pi b_c^2 \rho_i v_s \mathbf{v}_i$
	$\mathbf{F}_{orb} = 4\pi b_{\pi/2} \rho_i v_s \Gamma \mathbf{v}_i$
	with $v_s = \sqrt{v_i^2 + \frac{8T_i}{\pi m_i}}$

percent. Thus, most atoms are not in an ionized state and even though their cross sections are much smaller than those of ions, collisions with neutrals cannot be neglected in general. In particular, temperature gradients in the neutral gas are known to give rise to a thermophoretic force (see table 1 and [113–115]). Already temperature gradients of a few kelvin per centimeter are sufficient to compensate the gravitational force and levitate particles [114, 116]. The recent experiments of Carstensen *et al* [117] are another example. They showed that collisions of ions and neutrals can provide a sufficient transfer of momentum to set up a collective neutral gas motion which can drive dust particles. Thus, it is important to keep in mind that the neutral gas component might contribute more than just friction to dynamical processes in dusty plasmas.

### 2.5. Forces on dust particles

To understand dust confinement and dust dynamics, several forces are important (see table 1). For large particles, the gravitational force exceeds all other forces because it scales with the volume of the particles. Due to the high particle charge, Coulomb forces are important for both, particle confinement and particle interaction. Furthermore, thermophoretic forces due to temperature gradients in the neutral gas [113–115] and friction with ions and neutral gas [118] cannot be neglected for dust particles. While gravitational, Coulomb and thermophoretic forces as well as neutral gas friction are well understood, the ion drag force is still a subject of intensive research activity. There are several models for the ion drag force [78, 119–125], but a complete self-consistent model is not yet available. On the one hand, the self-consistent treatment of the charging and shielding problem of particles is aggravated by the requirement to include streaming ions and collisions. On the other hand, a correct description of the contribution of scattered ions to the momentum transfer is not trivial. Although the recent models reflect considerable progress, the debate on the description of the ion drag force has not finally settled. Only few experiments have studied the drag force quantitatively (e.g. [126–131]). The first experiments were performed in a parameter regime, where the influence of ion–neutral collisions during the scattering in the field of the dust particle cannot

be neglected. Hirt *et al* [130] presented the first dedicated ion drag investigations in a collisionless situation. The ion drag force and the collection radius  $b_c$  were measured for weak ( $\beta < 1$ ) and strong ( $\beta \gg 1$ ) ion–dust interaction. Here the momentum transfer is characterized by the scattering parameter  $\beta = e|\phi_{fl}|a/(m_i v^2 \lambda_D)$ , where  $m_i$  and  $v$  are the ion mass and velocity, respectively. For low values of beta ( $\beta < 0.2$ ) already the model of Barnes *et al* [78] was found to give a suitable description. At high ion energies, the collection of streaming ions was correctly described by the OML model [74]. For superthermal ion drifts ( $\beta = 50$ –122), however, the OML model predicts collection radii  $b_c > \lambda_D$ . In this case, the collection radius was overestimated by the model of Barnes. The critical parameter  $b_b$  from Khrapak *et al*'s model [122] gave a better description. Recently, Nosenko *et al* [132] repeated these experiments for  $\beta = 16$ –60 and found good agreement with a slightly modified Khrapak model.

### 2.6. Dust confinement

To confine dust particles inside a plasma, the gravitational force has to be balanced. Thus, dust confinement is typically achieved in the plasma sheath region above an electrode where strong electric fields are present [133]. The trapping of the dust particles in the horizontal direction is established by depressions of the electrode surface [134] or flat metal rings on the electrode [87]. However, this results in a very anisotropic confinement potential. The confinement in the vertical direction is much stronger and thus these dust clouds are mostly 2D systems which nevertheless can form highly ordered crystals with a hexagonal lattice structure [62–64]. Further, the supersonic ion flow toward the electrode is focused below each particle [105, 107–110]. In multilayer systems, the resulting positive space charge attracts particles in a lower layer. This process is responsible for chain formation observed in all dust clouds which are confined in the regions of strong electric fields, i.e. regions with strong ion flows (see e.g. figure 3(a)). This alignment vanishes if small particles and high gas pressures are used (figure 3(b)) [135–137]. However, extended homogeneous 3D plasma crystals cannot be generated this way and investigations of dust dynamics are not feasible due to strong damping.

To produce extended 3D dust clouds, different approaches were followed. Merlino and co-workers confined dust in a magnetized anodic plasma [141, 142] and investigated dust acoustic waves. In these experiments the dust confinement is achieved by a balance of electric field and ion drag forces in the horizontal direction [143] and ion drag, gravitation and electric fields in the vertical direction [144]. Barkan *et al* [145] calculated that the system can be in a strongly coupled state and recently Pilch *et al* [146] indeed observed well-ordered regions in these dust clouds, but their detailed structure is not yet understood.

To produce 3D plasma crystals, a number of experiments have been performed under microgravity conditions. These experiments have provided many interesting observations, e.g. of localized crystalline structures [147], of complex plasma boundaries [148, 149], of coalescence of complex plasma

fluids [150], of transport properties [151, 152] and of low frequency waves and instabilities [153–156]. However, the most striking observation was the formation of a dust free zone (void) at the center of the discharge [140, 147]. It was proposed that the ion drag force is responsible for the formation of these voids (figures 3(c) and (d)) [139, 157–159]. The combination of simulations [160–162], experiments [97, 114, 131, 163] and recent ion drag models [119–121] was able to verify this. Although it was shown very recently that a void closure can be achieved [164], the formation of void-free crystalline dust clouds is still an important issue.

### 2.7. Dust dynamics

Many investigations on complex plasmas focused on dynamic phenomena. New types of waves have been predicted and observed, e.g. dust acoustic waves [165], dust-ion acoustic waves [166, 167] and dust lattice waves [168, 169]. Many non-linear wave phenomena, e.g. shocks [155, 170–172] and Mach cones [173–176], were studied and the role of compressional and shear waves in solids and fluids has been discussed [177–180]. A recent review on this topic was published by Shukla and Eliasson [181]. Furthermore, the detailed investigations of the solid–fluid phase transition are certainly a highlight of complex plasma research [182–186]. Recently, a growing interest in liquid complex plasmas has been noted. Several investigations aim at a deeper understanding of transport and diffusion processes in strongly coupled liquids [151, 152, 187–192]. However, such dynamic properties were mostly studied in 2D complex plasmas.

## 3. Finite systems

Systems consisting of just a few particles are of special interest, because their structural and dynamical properties strongly depend on the precise number of particles. Already Thomson [196] investigated the structure of charged particle clusters in view of his atomic model. Although his results did not explain the structure of atoms, they mark the starting point for research on finite strongly coupled systems. Finite particle number effects have turned out to be of similar importance for the understanding of the structure of atomic nuclei. In the field of non-neutral plasmas Thomson's ideas have been developed much further [56]. Using the Penning and Paul traps [197] it was shown that the regime of strong coupling can be reached for laser-cooled ions [46, 198]. With refined experimental techniques the ions were found to arrange on nested shells [199] and for large ion clouds bcc order was observed, cf figure 4 [195, 200]. The same results were obtained with molecular dynamics simulations [56, 201, 202], and it should be noted that the particle arrangements, in particular those for closed shell configurations, are very similar to those of noble gas [203] and metal clusters [204]. This finding is a hint that geometric constraints might determine the structure of small systems to a large extent.

Nevertheless, when approaching large clusters the shell formation should vanish and a regular volume order should appear. This transition was predicted for ion clouds containing

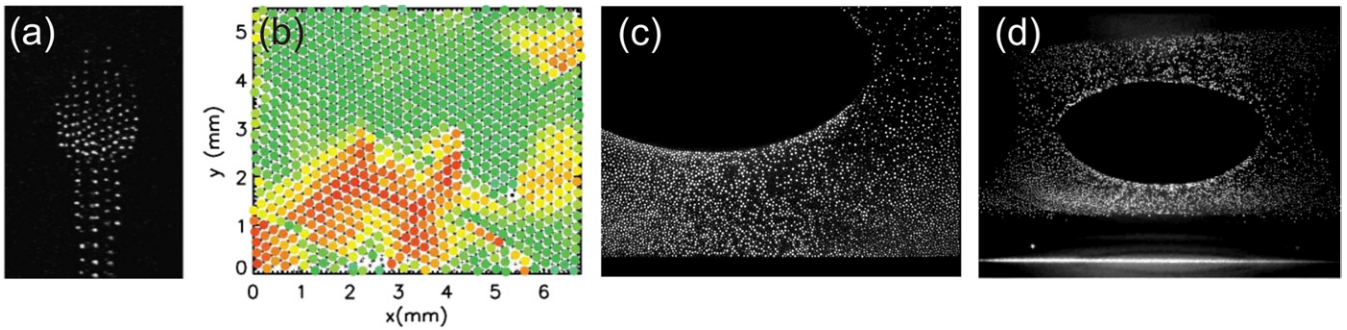


**Figure 3.** Examples for experimental realizations of 3D dust clouds. (a) Dust cloud in an inductively coupled rf-discharge. Note that the dust grains form vertical chains due to a strong vertical ion flow. (Reprinted with permission from [138]. Copyright 2000 Springer Science and Business Media.) (b) Structure of a multilayer crystal using small particles and high gas pressure to avoid chain formation. Coexistence of hcp (green) and fcc (red) lattices is observed. (Reprinted with permission from [137]. Copyright 2000 American Physical Society.) (c) Typical dust cloud under microgravity conditions. A dust free zone (void) establishes at the center of the discharge due to ion drag forces. (After [139, 140].) (d) If gravity is compensated by thermophoresis, similar voids are observed. (Reprinted with permission from [114]. Copyright 2002 American Physical Society.)

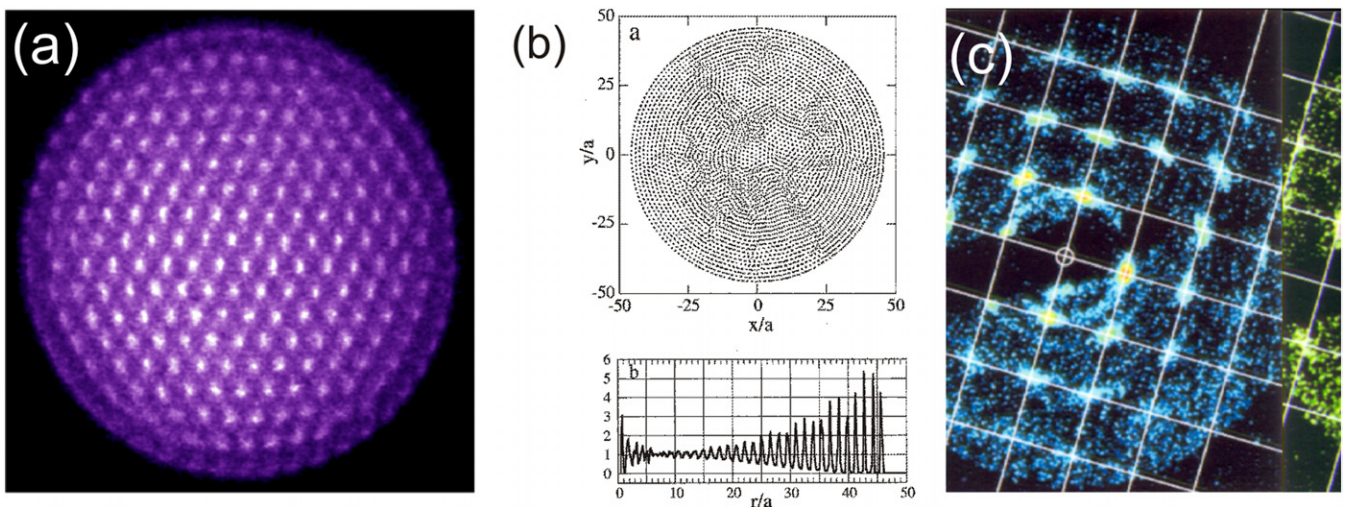


**Figure 4.** Structure of ion crystals. (a) Image of a small, spherical ion cloud ( $\sim 2000$  ions) in a Paul trap. The ions arrange in distinct shells. (After [193].) (b) MD simulation of a cloud with  $10^5$  ions reveals bulk order close to the center and shell formation outside. (Reprinted with permission from [194]. Copyright 2002 American Physical Society.) (c) Time-resolved Bragg diffraction pattern of a large ion cloud with a bcc lattice structure. (Reprinted with permission from [195]. Copyright 1998 American Association for the Advancement of Science.)

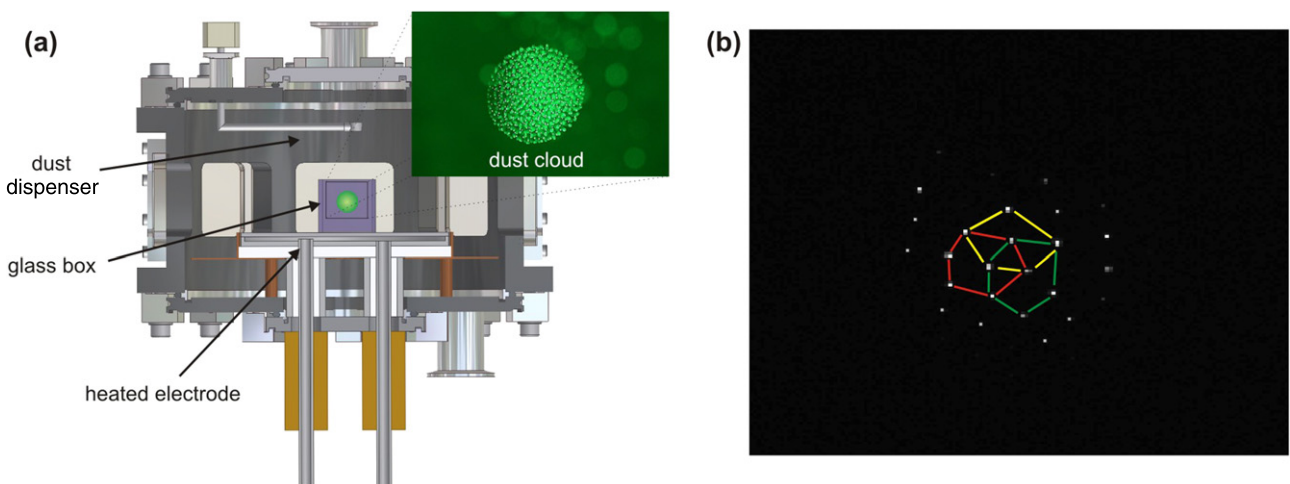


**Figure 5.** (a) Side view of the discharge arrangement for the Yukawa balls experiment. The lower electrode is heated ( $T < 90^\circ\text{C}$ ) and the vacuum vessel is grounded and kept at room temperature. The dust cloud is confined inside a glass cube where the upper and lower sides are left open. The inset shows an image of a large dust cloud which is 1 cm in diameter. (b) A thin slice at the front side of the cloud is illuminated. The particles basically arrange in a hexagonal lattice. (After [116].)

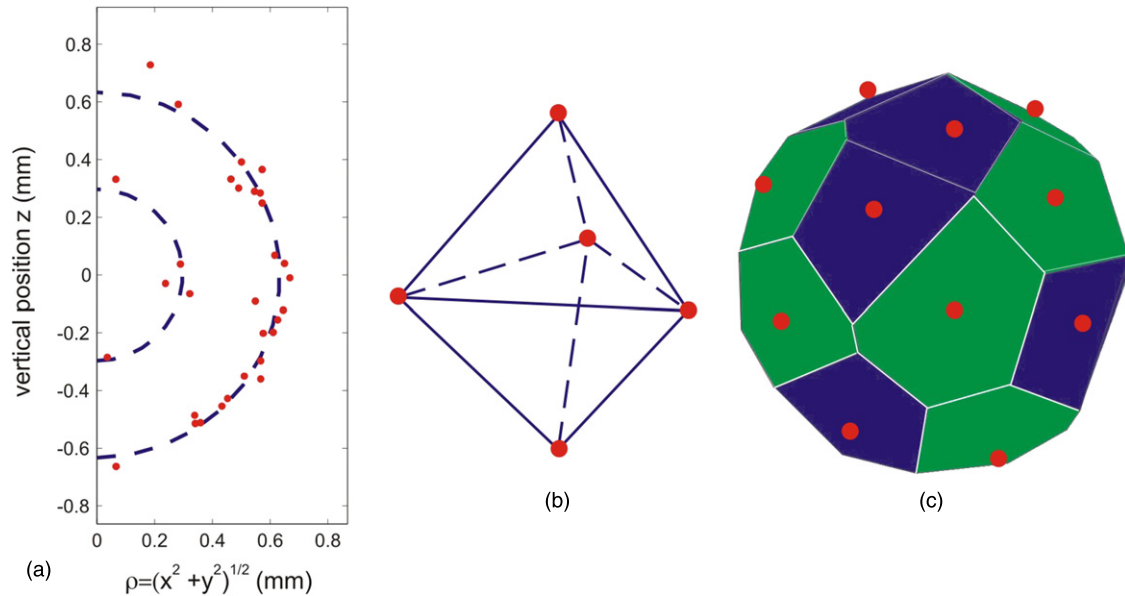


**Figure 6.** Structure of a Yukawa ball with  $N = 31$  particles observed experimentally. (a) Particle positions in cylindrical coordinates in the  $\rho$ - $z$  plane. The (red) dots are the average particle positions of a (5, 26) configuration, the dashed lines indicate the shells. (b) Structure of the inner shell. (c) Voronoi analysis of the outer shell with  $N_o = 26$ . Pentagons are dark (blue) and hexagons are bright (green). The particle positions are marked with dots. (Reprinted with permission from [216]. Copyright 2007 IOP Publishing.)

about  $10^4$  ions. However, recent experiments show that even small clouds ( $N \sim 10^3$ ) can show a bcc or fcc structure [193]. Further experiments investigated structural transitions due to resonant instabilities [205] and Coulomb bicrystals [206, 207]. In general, it can be stated that many theoretical predictions [56] for these systems are not yet verified by experiments, e.g. the size dependence of the melting process. The main reason for this is that the ion clouds are about 20 times smaller than complex plasma clouds with the same particle number and that the ion dynamic is too fast to track individual ions. Hence, these experiments are restricted to the analysis of the average structure of ion clouds. However, Juan *et al* [208] demonstrated that such experiments are generally possible in complex plasmas. Klindworth *et al* were able to show that the structural and dynamical properties of finite 2D clusters strongly depend on the particle number [209]. Further experiments and simulations treated normal modes [210], phase transitions [211] and structural properties of these systems [212, 213].

In 3D, interesting observations were reported by Annaratone and co-workers [214, 215]. They observed spherical dust clouds with less than 50 particles in a secondary discharge in front of an adaptive electrode. Unfortunately, these clouds are rather in a liquid state and their confinement is not yet understood. Similar dust clouds but in a well-defined confinement were generated by Arp *et al* [116]. Using thermophoresis to balance gravity and a glass box to generate radial electric fields, they managed to create an isotropic parabolic confinement potential, cf figure 5. Inside this trap the dust particles were found to form spherical dust clouds. Figure 6(a) visualizes the typical structure of an experimentally generated so-called Yukawa ball. Using cylindrical coordinates,  $z$  and  $\rho = \sqrt{x^2 + y^2}$ , a formation of shells is clearly observed. The inner shell consists of 5

particles whereas 26 particles form the outer shell. While the inner shell is a symmetric double tetrahedron (figure 6(b)) which represents a typical close-packed structure, the Voronoi-analysis of the outer shell shows a pattern of hexagons and pentagons (figure 6(c)). Thus, Yukawa balls are in a crystalline state and the particle arrangement is similar to the one in ion crystals.

## 4. Structure of plasma crystals

After having discussed the basic issues of dusty plasma experiments we will now concentrate on the results in the strong coupling regime. The large amount of work in this field does not allow for a comprehensive presentation of all results and even of the main systems. We will, therefore, focus on one particular system—finite spherically confined dusty plasmas in the liquid and crystal states. For this system we will discuss a variety of properties in close comparison between experiment and theory.

### 4.1. Theoretical models

We now turn to a theoretical analysis of the structure of plasma crystals and start by analyzing the plasma conditions. First, due to the large size and mass of the dust particles quantum effects are irrelevant. This holds not only for the presently used temperatures but also for cryogenic conditions with temperatures in the micro-kelvin range unless particles in the sub-nanometer range are being used. But in that case, the advantage of achieving highly charged particles will be lost. Thus for this classical system, in principle, an exact simulation approach is possible. Such approaches which are based on particle in cell (PIC) simulations have in fact been developed by Matyash and others but they are presently capable of treating

only a very few dust particles in the plasma. These difficulties are caused by the second peculiarity—the embedding of the dust particles into a partially ionized plasma consisting of neutral gas molecules, ions and electrons, all of which have a mass which is at least 10 orders of magnitude smaller. This leads to an essential decoupling of the dust particle motion from that of the plasma—in many cases the plasma can be assumed quasi-stationary and instantaneously following the motion of the heavy particles. Therefore, instead of simulating the complex plasma exactly it is possible to develop hybrid concepts (see e.g. [217] and references therein).

The third peculiarity of dusty plasmas is that strong correlations appear asymmetrically. While the dust component may be very strongly correlated with  $\Gamma_d \gg 1$ , the correlations of the electron and ion subsystems are normally very small,  $\Gamma_{e,i} \ll 1$ , and also the coupling of the dust to electrons and ions is weak (the coupling parameters associated with the average dust–electron and dust–ion interaction are small). This allows one to develop effective one-component plasma (OCP) models where the dust is treated exactly whereas the properties of the lighter components enter via several input parameters. The fourth aspect is that the dusty plasma is in a non-equilibrium state which can be considered stationary: electrons and ions counterstream between the electrodes and (in particular electrons) attach to the surface of the dust particles, see the discussion in section 2. A simplified model which treats the streaming electrons and ions within linear response and computes the dynamically screened potential  $V$  of the dust particles was developed by Joyce and Lampe (see [218, 219] and references therein). They derived an anisotropic and non-monotonic (wake) potential around a dust grain which explains many of the unusual observations such as effective dust–dust attraction, cf section 2, as well as the control of dust crystallization by variation of the neutral gas pressure.

**4.1.1. Langevin molecular dynamics simulations.** In the following we will take advantage of the peculiarities of dusty plasmas mentioned above. For simulations of spherical dust crystals which are formed in the plasma bulk, electron and ion streaming are of minor importance, so dynamical screening effects can be neglected. Then the simplest effectively one-component model is given by the Hamiltonian (1) for the dust particles where the properties of the light plasma species are included into the pair interaction potential  $V$  and the confinement potential  $U$ . For the interaction potential  $V$ , an isotropic Yukawa potential (see equation (7)) can be used as will be verified by comparisons with the experimentally observed crystal structures below. On the other hand, the interaction of the dust particles with the dominant species, the neutral gas, can be treated as in standard Brownian motion: by a simple Stokes-type friction (see table 1) together with a noise term,

$$m\ddot{\mathbf{r}}_i(t) = \mathbf{F}_i(t) - \nu m\dot{\mathbf{r}}_i + \mathbf{y}_i(t), \quad i = 1, \dots, N, \quad (8)$$

$$\langle \mathbf{y}_i \rangle = 0, \quad \langle y_{i\alpha}(t)y_{j\beta}(t') \rangle = 2D\delta_{i,j}\delta_{\alpha,\beta}\delta(t-t'),$$

$$\alpha, \beta = x, y, z,$$

which models the random collisions of dust particles with neutral gas atoms. If the latter are in thermodynamic

equilibrium with a temperature  $T_n$ , which is normally the case, the particles will relax toward a Maxwellian velocity distribution with the same temperature, and the random force amplitude  $D$  is determined by the fluctuation–dissipation relation,  $D = mk_B T_n \nu$ . The force  $F_i = -\nabla_i U - \nabla_i V$  is the total force on the  $i$ th particle due to the external potential and all other dust particles.

Solving this set of equations yields a first-principle simulation (Langevin molecular dynamics, LMD) for the dust particles which does not make any approximation with respect to the coupling strength. This approach thus allows one to systematically study the details of the dust ensemble in the whole parameter space, including the strongly coupled liquid and crystal regimes. A second first principle approach which provides the thermodynamic properties is Monte Carlo simulations with the Hamiltonian (1). This provides the crystal structures and melting points, but cannot reveal dynamic properties. We will discuss examples of such simulations in section 4.3.

**4.1.2. System of units.** For the theoretical and numerical analysis it is useful to define proper dimensionless quantities based on physical length, time and energy scales,  $r_0, t_0, E_0$ .

- (i) For macroscopic systems, we will use, as the length scale, the Wigner–Seitz radius,  $r_0 = \bar{r}$  and the associated energy scale  $E_0 = Q^2/r_0$ . The characteristic time scale is the inverse plasma frequency,  $t_0 = \omega_p^{-1}$ , and frequencies and damping constant  $\nu$  are given in units of  $\omega_p$ .
- (ii) For finite systems in a spherically symmetric harmonic trap potential,  $U(r) = m\omega^2 r^2/2$ , it is convenient to use

$$r_0 = (2Q^2/m\omega^2)^{1/3}, \quad (9)$$

$$E_0 = (m\omega^2 Q^4/2)^{1/3},$$

where  $r_0$  is the stable distance of two particles with Coulomb repulsion in a harmonic trap and  $E_0$  is their total energy. A natural unit of time is the inverse trap frequency  $t_0 = \omega^{-1}$  whereas frequencies and the dissipation constant  $\nu$  are given in units of  $\omega$ .

## 4.2. Pair distribution function of a strongly coupled plasma

For a quantitative analysis of the correlation effects a variety of quantities can be used, besides the coupling parameter  $\Gamma$ , equation (2). Spatial correlations and formation of long-range order are well characterized by the pair distribution function  $g(r)$ ,

$$g(r) = \frac{V}{N(N-1)} \left\langle \sum_i \sum_{j \neq i} \delta(|\mathbf{r} - \mathbf{r}_{ij}|) \right\rangle, \quad (10)$$

which is normalized to the system volume,  $\int d^3r g(r) = V$ , and represents the probability of finding an arbitrary particle pair at a distance  $r$ . In dusty plasmas, this quantity is not only easily computed from simulations but also directly measured from the available particle positions. The function  $g(r)$  is straightforwardly computed within a molecular dynamics simulation by analyzing all pair distances  $r_{ij}$ . A simulation example is shown in figure 7 for the case of an OCP monolayer at three different coupling strengths. The function evolves

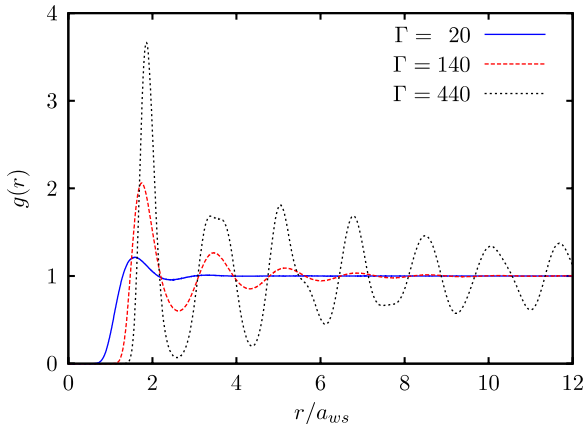


**Figure 7.** Pair distribution function of a one-component Yukawa plasma ( $\kappa a_{ws} = 2.0$ ) in two dimensions. The curves correspond to the solid phase, ( $\Gamma = 440$ ), the strongly ( $\Gamma = 140$ ) and the moderately coupled liquid phase ( $\Gamma = 20$ ). For an ideal system,  $g(r) \equiv 1$ . Length unit is the Wigner–Seitz radius  $a_{ws}$ .

from a constant,  $g(r) = 1$ , in an ideal plasma, to a curve with a minimum around zero (‘correlation hole’) at  $\Gamma > 0$ . With increasing coupling, first, short-range ordering appears, cf the curve for  $\Gamma = 20$ , until long-range order emerges, which corresponds to a crystalline state. Note that for finite systems the pair distribution function decays to zero, for distances of the order of the system size, see figure 10.

There exist many other quantities well suited to characterize the many-particle effects and the spatial ordering, including the static structure factor (essentially the Fourier transform of  $g(r) - 1$ ). Further quantities suitable for characterizing finite spherical crystals will be discussed in section 4.3. The experiments with dusty plasmas directly allow one to measure the pair distribution function and to compare with theoretical approaches. An example for a measurement of a spherical plasma crystal is presented in figure 10.

#### 4.3. Spherically confined crystals: Yukawa balls

The spherical crystals (Yukawa balls) consist of a finite number  $N$  of dust particles where  $N$  can be varied between one and a few thousand. This gives access to a whole new field of strongly correlated systems in which finite size effects play a crucial role. Even though these systems are classical, they have properties very similar to atoms and nuclei—they can be in a variety of stationary states characterized by a well-defined total energy. Ground state and metastable states can be realized in experiments, see below, and are easily studied with simulations and analytical models.

As shown by the experiments, see section 3, the dust particles forming the crystal are confined by an isotropic and nearly harmonic potential,  $U(r_i) = m\omega^2 r_i^2/2$ . This crystal is formed in the plasma bulk so that the dust–dust interaction is well approximated by a Yukawa potential (7). Note that in a harmonic potential, the absolute strength of the confinement (i.e. of  $\omega$ ) has no influence on the plasma state. An increase in  $\omega$  leads only to a reduction in the interparticle distances, as can be seen from equation (9) for the case of two particles. The same is true for Yukawa systems [220].

**4.3.1. MD results for the ground state.** With these input parameters, the structure of the Yukawa balls is easily obtained by simulations solving the equations of motion (8) without the dissipation and stochastic force terms (MD). Since the screening parameter is difficult to measure accurately it is used as a free parameter. Based on the experimental estimates, the Yukawa balls are strongly correlated, with  $\Gamma \gtrsim 500$ . Thus the observed crystal structure should be close to the ground state. The classical ground state of system (1) is obtained by neglecting the kinetic energy and by finding the absolute minimum of the total potential energy. The simulations are conceptually very simple: one starts with a random particle configuration and proceeds with slow ‘cooling’ (reduction of the particle velocities) until the desired temperature—zero for the ground state—is reached, so-called ‘simulated annealing’. Nevertheless, there are many caveats: there exists no computational scheme which will with certainty lead to the ground state, in a finite time. With high probability a simulation will end up in a local minimum of the potential energy, rather than in the absolute minimum. Therefore, simulations have to be repeated sufficiently frequently, typically several thousand times. Also, rapid cooling will not lead to the ground state but rather to metastable or glass-like states. On the other hand, very slow cooling will be very inefficient, and one has to find an optimal time step.

Let us summarize the results: at  $T = 0$  the dust particles form narrow concentric shells which agrees with the measurements, cf figure 6. Ground state and metastable states are characterized by a definite set of shell occupation numbers  $\{N_s\}$ . With increasing cluster size, particles continuously populate a shell until its capacity is reached (so-called ‘magic’ clusters) and a new shell forms. Shell closures have been investigated in detail for spherical Coulomb systems by Hasse and Avilov [201], Tsuruta and Ichimaru [202], Ludwig *et al* [221] and many others. The first shell is closed for  $N = 12$ , the second for  $N = 57$  and again for  $N = 60$  [202]. The closure of the third and fourth shells is observed for  $N = 154$  [221, 222] and  $N = 310$  [220], respectively.

However, the shell occupation numbers are not sufficient to fully characterize the stationary state. Clusters with the same occupation numbers  $\{N_s\}$  can be in one of several configurations differing by the intra-shell symmetry. This ‘fine structure’ was investigated in detail in [221] where it was observed that the ground state is characterized by the highest intra-shell symmetry. Each shell is characterized by a combination of six-fold and five-fold symmetries, i.e. particles have, respectively, six and five nearest neighbors (other symmetries are also observed but less frequently), known as Euler’s problem, in agreement with the measurements, cf figure 6. A prominent example is the cluster with  $N = 12$  particles which forms a single shell with 4 (8) particles having 6 (5) nearest neighbors. Another example is shown in figure 8 depicting the ground and the first excited states for  $N = 17$ , both having the same shell configuration and the same number of hexagons (4) and pentagons (12), but differing in their arrangement.

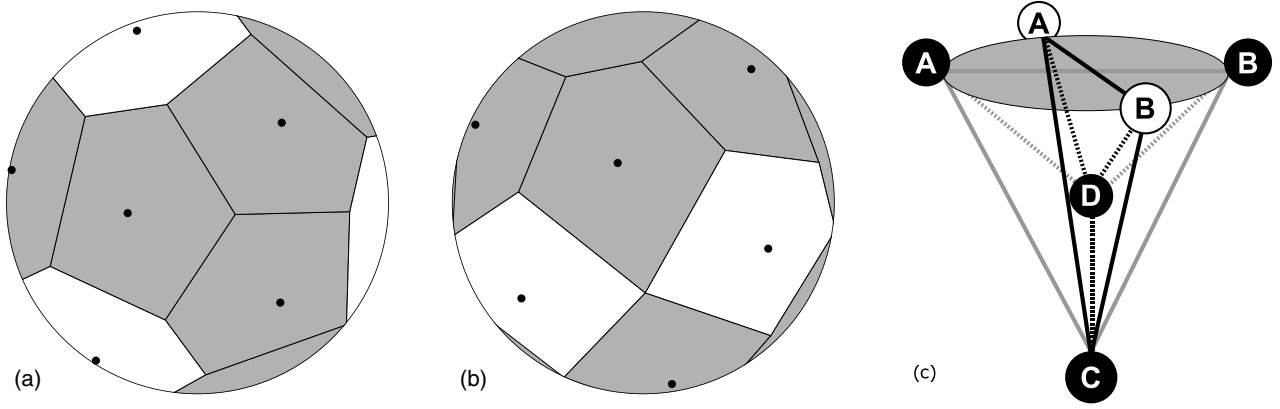


**Figure 8.** Voronoi construction for the cluster  $N = 17$ —the two energetically lowest states with shell configuration  $N_s = \{1, 16\}$  are shown. White (gray) areas are hexagons (pentagons)—indicating the number of nearest neighbors of the corresponding particle (black dot): (a) ground state, (b) first excited (‘fine structure’) state, (c) arrangement of the four particles surrounded by hexagons—the two states differ by rotation of the edge  $AB$ , black [white] circles correspond to case (a) (b). (Reprinted with permission from [221]. Copyright 2005 American Physical Society.)

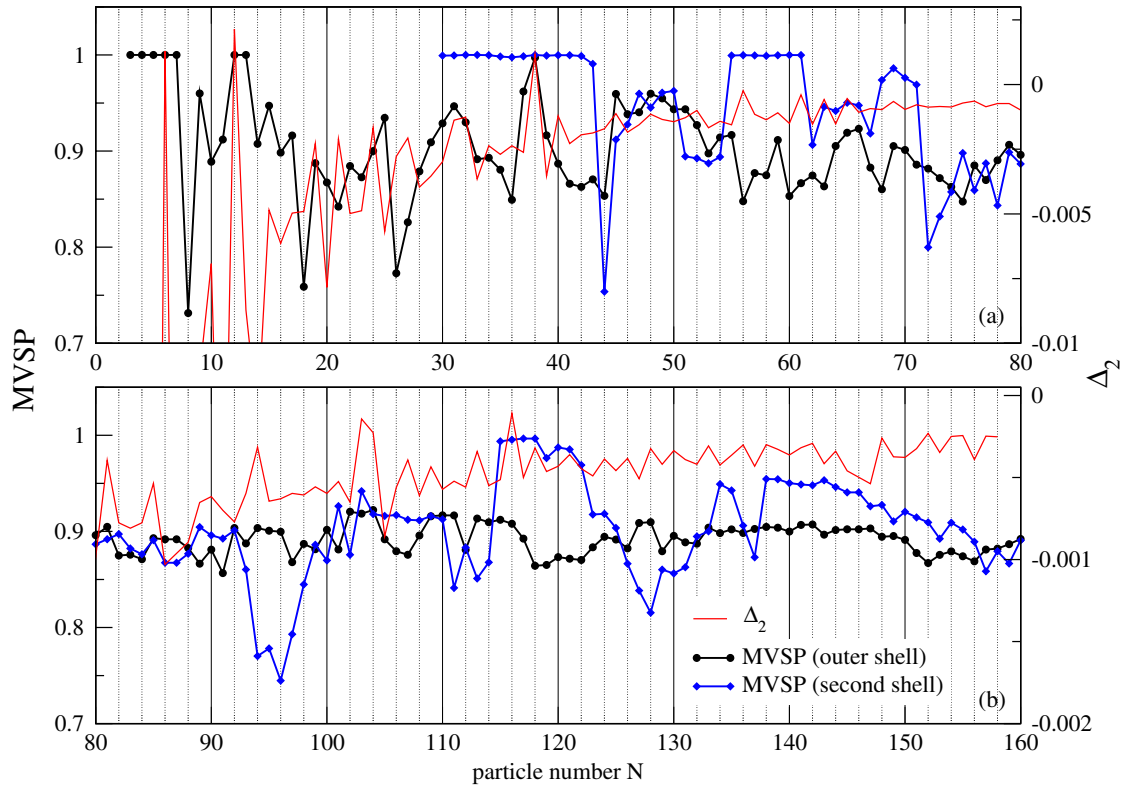


**Figure 9.** Binding energy  $\Delta_2$  (right axis) and MVSP (left axis), equation (12), for the two outermost cluster shells: (a)  $N \leq 80$ , (b)  $80 \leq N \leq 160$ . (Reprinted with permission from [221]. Copyright 2005 American Physical Society.) (Color online.)

The strong correlation between cluster stability and symmetry is demonstrated in figure 9 where the binding energy  $\Delta_2$  and the mean Voronoi symmetry parameter (MVSP),

$$\Delta_2 = E(N+1) + E(N-1) - 2E(N), \quad (11)$$

$$\text{MVSP} = \frac{1}{N^{\text{shell}}} \sum_{M=4,5,6} N_M G_M, \quad N_4 + N_5 + N_6 = N^{\text{shell}}, \quad (12)$$

$$G_M = \frac{1}{N_M} \sum_{j=1}^{N_M} \frac{1}{M} \left| \sum_{k=1}^M e^{iM\theta_{jk}} \right|, \quad (13)$$

are plotted together for clusters with  $N$  from 1 to 160. The MVSP is the weighted (by the corresponding number  $N_M$  of particles) average of the bond angular order parameters  $G_M$  within a shell. Here  $N_M$  denotes the number of all particles  $j$  in the shell, each of which is surrounded by a Voronoi polygon of order  $M$  ( $M$  nearest neighbors) and  $\theta_{jk}$  is the angle between the  $j$ th particle and its  $k$ th nearest neighbor. For example, a value  $G_5 = 1$  ( $G_6 = 1$ ) means that all pentagons (hexagons) are perfect, the magnitude of the reduction of  $G_M$  below 1 measures their distortion. For the cases included in figure 9 only the symmetries with  $M = 4, 5, 6$  occur

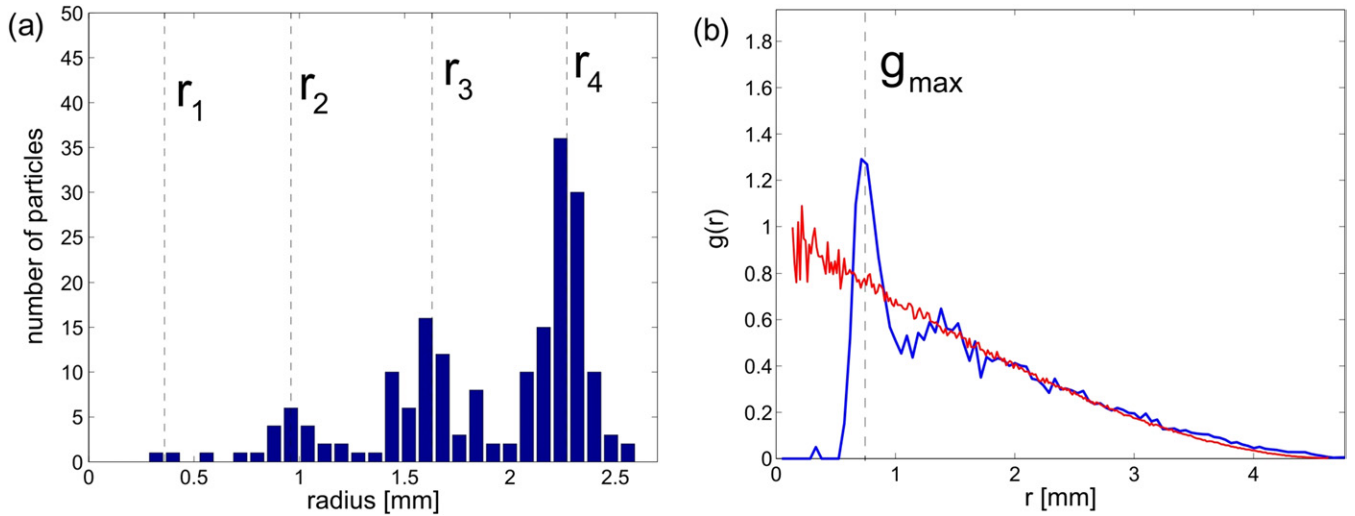


**Figure 10.** Experimental results for a Yukawa ball with  $N = 190$  particles: (a) Radial particle distribution, clearly indicating formation of four concentric shells and (b) the associated pair distribution function, indicating a strongly correlated liquid-like state. The monotonically decreasing (red) curve shows the pair distribution function for a random distribution of particles in a spherical cloud with the same volume. (Reprinted with permission from [223]. Copyright 2005 American Institute of Physics.) (Color online.)

[221]. Magic clusters—as in the case of noble gas atoms or magic nuclei—have a particularly high binding energy (high stability) and a high symmetry; prominent examples are  $N = 12, 38, 103, 116$ . Note that these magic numbers differ from those in nuclei or neutral gas clusters due to the different pair interaction potentials.

Finally, small clusters,  $N \leq 12$  have a particularly symmetric arrangement—they form platonic bodies. These reappear in the core of larger clusters, cf figure 6. With increasing cluster size the competition between bulk order and spherical order due to the trap becomes more pronounced and for  $N \gtrsim 10^4$ , the bulk order begins to prevail in the core, as was shown by Totsuji *et al* [194].

**4.3.2. Comparison with experiments: screening dependence of the ground state.** The high quality of the dusty plasma experiments makes it possible to directly compare the measured cluster configurations with the above theoretical predictions. In figure 10 experimental results for a Yukawa ball with 190 particles are shown. The radial density profile (left) clearly confirms the formation of concentric shells. At the same time, the pair distribution function (right) signals the emergence of a quasi-long-range order. The decay is a consequence of the finite cluster size and is also present in an ideal (non-interacting) cluster, cf figure 10.

The shell configurations for a large number of Yukawa balls containing 100–500 particles were reported in [220], see figure 11. The overall trend observed in the simulations and in the experiment is an increase in  $N_s$  proportional to  $N^{2/3}$ . However, the experimentally determined occupation numbers  $\{N_s\}$  show small deviations from the theoretical results for Coulomb clusters of about 5–10%. The authors could show that this is not due to statistical errors but is a systematic difference which is explained by screening of the interaction. In fact, screening leads to a reduced repulsion—the clusters shrink and, at the same time, it is energetically favorable for the

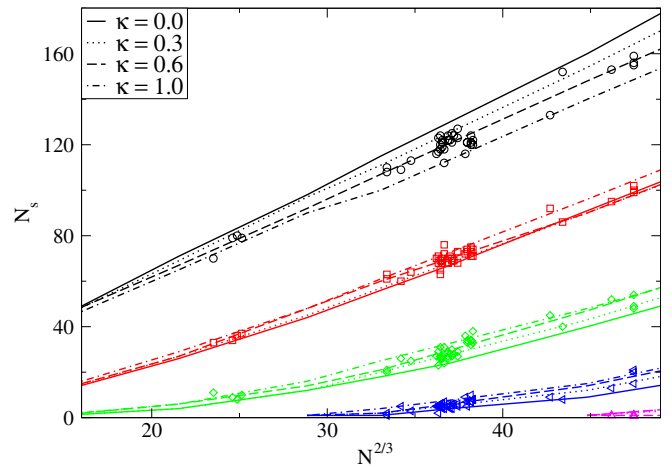


**Figure 11.** Experimental (symbols) and theoretical (lines) shell population  $N_s$  of the ground states versus system size. The MD results are obtained for different screening parameters  $\kappa$  ( $\kappa$  is given in units of  $r_0$ ) and show that the particles redistribute toward inner shells with increased  $\kappa$ . Good agreement is observed for  $\kappa r_0 = 0.6$ . (Reprinted with permission from [220]. Copyright 2006 American Physical Society.) (Color online.)

particles to increasingly occupy inner shells. Results for  $\{N_s\}$  for several values of  $\kappa$  are shown in figure 11. A comparison with the experiments allows one to deduce an average value of the Debye screening length in the experiment of  $\lambda_D/a \approx 1.5$  where  $a$  is the mean interparticle distance (this corresponds, in dimensionless units, to  $\kappa r_0 = 0.6$ ), in good agreement with other measurements.

Thus these experiments confirmed the existence of an effective screened interaction between two dust particles—which is a qualitative difference compared with ultracold ions in traps. Subsequently there have been numerous studies of the properties of finite spherical Yukawa plasmas and of their dependence on the screening strength. Baumgartner *et al* have

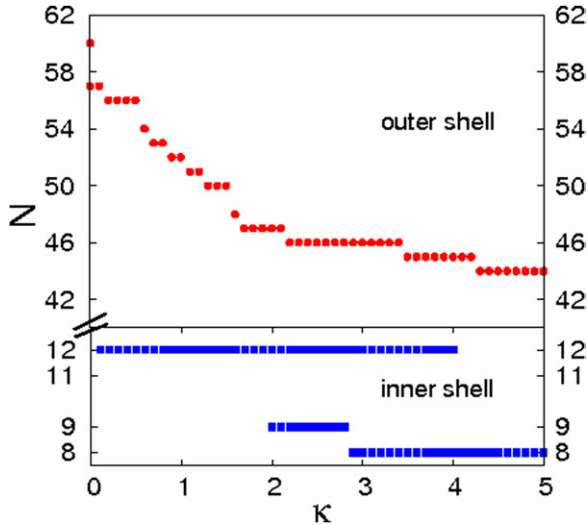


**Figure 12.** Shell closures for Yukawa ball ground states.  $N$  denotes the last cluster with only one shell (lower curve) and two shells (upper curve) for the given value of  $\kappa$  (in units of  $r_0^{-1}$ ). The  $N + 1$ st particle will be located at the trap center, opening a new shell. Note the re-entrant shell closures for the outer shell (for  $\kappa = 0$ ) and the first shell (for  $2.0 \leq \kappa \leq 4.0$ ). (Reprinted with permission from [224]. Copyright 2008 IOP Publishing.)

computed all shell configurations for  $N \leq 60$  in a broad range of  $\kappa$  [224]. The first observation is that the magic clusters (clusters with a closed shell) with increased  $\kappa$  move to lower  $N$ . This is shown in figure 12. While, overall, an increase in  $\kappa$  leads to an increased occupation of inner shells, there exist a number of interesting anomalies: (1) upon  $\kappa$  increase two particles may move to (one of) the inner shell(s) at once, (2) when the particle number is increased by one, at fixed  $\kappa$ , in some cases one particle moves from the inner to the outer shell and (3) at very large  $\kappa$  there exist cases of re-entrant shell fillings: one particle returns from the inner to the outer shell. These anomalies are, in most cases, dictated by symmetry properties of the corresponding state which allow one to lower the total energy.

**4.3.3. Shell models.** The observed shell structure suggests that the main crystal properties can be obtained from simpler shell models. Such a model assumes that the particles are homogeneously distributed along  $L$  concentric shells with zero width. The first shell model was proposed by Avilov and Hasse for ion crystals (pure Coulomb interaction) [201] and was improved by Tsuruta and Ichimaru [202] who approximately included correlation effects. Kraeft and Bonitz further improved this model and presented detailed comparisons with MD simulations [225]. They gave the following form of the total energy per particle (they also subtracted a term  $\frac{9}{10}N^{2/3}$  which accounts for a possible neutralizing background but can be omitted for our present discussion of the shell structure):

$$\frac{E_{\text{model}}(N)}{N(Ze)^2/r_0} = 2^{1/3} \sum_{v=1}^L \frac{N_v}{N x_v} \times \left( \frac{N_v - \epsilon \sqrt{N_v}}{2} + \sum_{\mu < v} N_\mu + \zeta + \frac{1}{2} x_v^3 \right), \quad (14)$$

where  $\zeta = 0$  or 1 (accounting for the possibility of a particle sitting exactly at the trap center) and  $x_\mu$  is the radius of the shell  $\mu$  in units of  $r_0$ . Here, the first term (proportional to  $N_v^2$ ) is related to the surface energy of a spherical capacitor of radius  $x_v$ , containing  $N_v$  charges, with  $E_{\text{surf}}(N) = [N(N-1)e^2]/(2x_v)$ . The sum over  $\mu$  accounts for the electrostatic interaction of the shell  $v$  with all inner shells whereas the  $x_v^3$  contribution describes the confinement energy. This model, without the term proportional to  $\epsilon$ , can be rigorously derived from a mean-field theory [226] which is discussed in section 4.4. The term proportional to  $\epsilon$  takes into account the discreteness of the particles by excluding a certain area around each particle from the available shell area and thus accounts for intra-shell correlations. The cluster configuration can now be derived simply by an optimization procedure searching for those shell populations and radii which minimize the total energy (14) which is much simpler than to solve the exact problem. While this yields the correct qualitative trend, with  $\epsilon = 0$  [201] there are large quantitative deviations from the MD simulation results [225]. Using  $\epsilon$  as an additional free parameter allows one to reduce the deviations from the exact ground state energy to (1–2)% [225]. The resulting values for  $\epsilon$  were slightly above 1 and converged to  $\epsilon = 1.104$  for large  $N$ , a result which could be recently derived from the Thomson model by Cioslowski [227, 228].

For Yukawa balls the situation is more complex. A mean-field-type model ( $\epsilon = 0$ ) was recently obtained by Totsuji *et al* [229] and derived from continuum theory, cf section 4.4, by Henning *et al* [226],

$$E_{\text{model}}(N; \kappa) = \sum_{v=1}^L N_v \left\{ \frac{\alpha}{2} R_v^2 + Q^2 \frac{e^{-\kappa R_v}}{R_v} \times \left( \frac{\sinh(\kappa R_v)}{\kappa R_v} \times \frac{N_v - \epsilon_v(N, \kappa) \sqrt{N_v}}{2} + \zeta + \sum_{\mu < v} \frac{\sinh(\kappa R_\mu)}{\kappa R_\mu} N_\mu \right) \right\}. \quad (15)$$

One readily confirms that this result includes the Coulomb case. Model (15) differs from [226, 229] by the additional correlation corrections which generalize the Coulomb expression (14). This model was used in [230] and optimized to minimize the total energy. A detailed comparison with exact results showed that the model with  $\epsilon = 0$  performs rather poorly. In contrast, allowing for correlation corrections  $\epsilon_v$  which are different for different shells gives rise to an accuracy of about 5% for the shell populations compared to experiment and simulations. Such shell models are a valuable complement to simulations since they allow for insight into the structure of the Yukawa balls.

#### 4.4. Radial density profile of Yukawa balls

The experimental data suggest that the mean density in Yukawa balls is distributed inhomogeneously. This is in striking contrast to a system of charged particles (with Coulomb interaction): as is known from electrostatics, a homogeneously charged sphere produces a parabolic electrostatic potential  $\phi_{e1}$  in its interior, cf figure 13. Vice versa, a parabolic confinement will give rise to a homogeneous distribution of particles with Coulomb interaction. However, this is not the case for particles

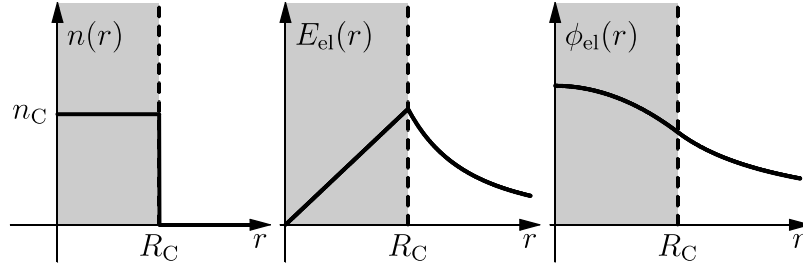


**Figure 13.** A homogeneously charged sphere (Coulomb interaction, density  $n(r)$ ) with radius  $R_C$  produces inside a linear field  $E_{el}$  and a parabolic potential  $\phi_{el}$ .

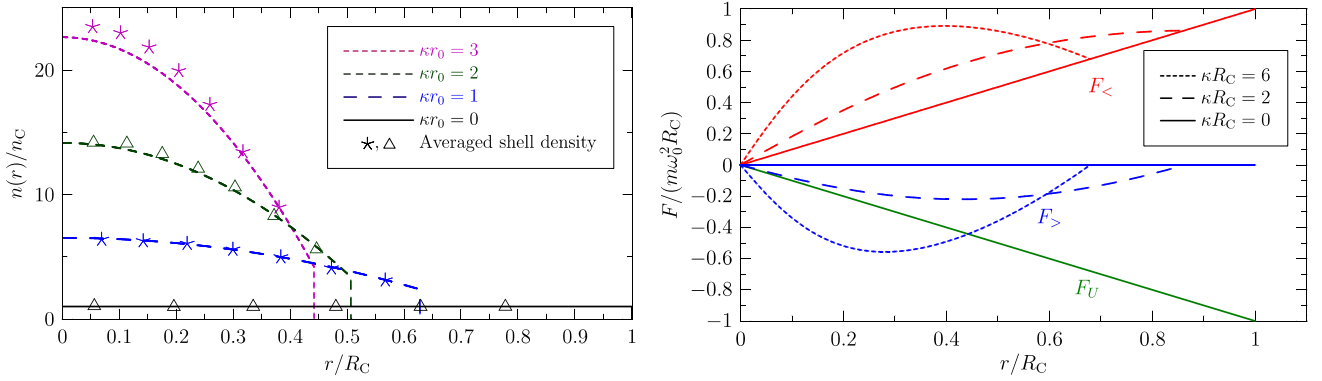


**Figure 14.** (Left) Mean radial density profile in mean-field approximation, equation (19), lines, compared with exact result (symbols), for four different screening parameters. (Right) Radial profile of the force contributions on a particle at radial position  $r$  for three screening parameters.  $F_U$  is the force produced by the confinement and  $F_<$  ( $F_>$ ) the force from all particles inside (outside) the radius  $r$ . (Color online.)

with Yukawa interaction. The corresponding radial profile has been computed by Henning *et al* [226]. The derivation uses a classical version of density functional theory: the ground state total energy is written as a (unique) functional of the density profile  $n(r)$ :

$$E[n] = \int d^3r u(r), \quad (16)$$

$$u(r) = n(r) \left\{ U(r) + \frac{N-1}{2N} \int d^3r_2 n(r_2) \frac{Q^2}{|r-r_2|} e^{-\kappa|r-r_2|} \right\} + u_{corr}, \quad (17)$$

where the terms on the right denote the confinement energy density, the mean-field contribution and the density of the correlation energy. The ground state density profile is obtained from minimizing the total energy  $E$ , i.e. from the variational problem  $0 \stackrel{\cdot}{=} \delta E[n]/\delta n(r)$  under the constraint  $\int d^3r n(r) = N$ . The solution for a general anisotropic confinement  $U(r)$  in mean-field approximation ( $u_{corr} \equiv 0$ ) is given by [226]

$$4\pi Q^2 \frac{N-1}{N} n(r) = (\Delta - \kappa^2)U(r) + \kappa^2\mu, \quad (18)$$

where  $\mu$  is a Lagrange multiplier (chemical potential) assuring the normalization.

For the case of Yukawa balls, we use an isotropic harmonic potential,  $U(r) = m\omega^2 r^2/2$ , and equation (18) yields the explicit result (we define  $\tilde{Q}^2 = Q^2/(m\omega^2)$ )

$$n(r) = \frac{N}{4\pi(N-1)\tilde{Q}^2} \left( c - \frac{\kappa^2 r^2}{2} \right) \Theta(R-r), \quad (19)$$

$$c = 3 + \frac{R^2 \kappa^2}{2} \frac{3 + \kappa R}{1 + \kappa R}.$$

The density drops to zero at a finite radius  $R(N, \kappa)$  which follows from the normalization, yielding the following equation:

$$\tilde{Q}^2(N-1) + \tilde{Q}^2(N-1)\kappa R - R^3 - \kappa R^4 - 2\kappa^2 R^5/5 - \kappa^3 R^6/15 = 0, \quad (20)$$

which has a single real positive solution  $R(\kappa, N)$  [226]. The result for the density profile is shown in figure 14. As expected, for a Coulomb system ( $\kappa = 0$ ), a constant profile is observed which terminates at a finite radius  $R = R_C = [(N-1)Q^2/(m\omega^2)]^{1/3}$ , with a step. With increased screening, the cluster is compressed due to the weakened interparticle repulsion. This is clearly seen by the reduction in  $R$ . Furthermore, the profile is not constant anymore but decreases parabolically towards the edge where the decrease becomes steeper with increasing  $\kappa$ , cf equation (19).

This density profile provides a global minimum to the total energy (16) and, at the same time, it assures stability of the cluster locally, i.e. for any  $r$  simultaneously. In fact, computation of the gradient of the total potential energy yields the force on the particles, cf right part of figure 14. There are three contributions to the force: the first,  $F_U$ , results from the confinement and is directed inward. On the other hand, the particles themselves produce a repulsive force. For a particle located at any given radius  $r \leq R$  there is a force  $F_<$  from all particles located inside a sphere of radius  $r$  which acts toward the edge. In the Coulomb case, these two forces are both linear functions and exactly balance each other, for any  $r$ , see the solid lines in figure 14. Obviously, there is no force from the particles located at radii larger than  $r$ , i.e.  $F_> \equiv 0$ , which is nothing but the Faraday cage effect. The situation

is completely different in the case of a screened interaction,  $\kappa \neq 0$ . In this case, there is no Faraday cage effect—particles located outside a given radius produce a substantial inward force which adds to the force  $F_U$ . Thus, stability requires an increased (compared with the Coulomb case) force  $F_<$ . Due to the shorter range of the interaction, the plasma can accomplish this only by strongly increasing the density toward the center.

Finally, it is interesting to compare the results of this mean-field model for the density profile with the exact results which are shown by the symbols in the left part of figure 14. For comparison, the exact ground state profile which is characterized by a radial modulation (shell structure) has been averaged over radial intervals, for details, see [226]. The agreement is surprisingly good, at least for  $\kappa r_0 \leq 2$ . For larger  $\kappa$ , there are growing deviations in the central part of the cluster which are due to the neglect of the correlation energy  $u_{\text{corr}}$ . In fact, it was shown by Henning *et al* [231] how to include correlations in a local density approximation. The results were in excellent agreement with the simulations for  $\kappa r_0 \geq 2$  but they are less accurate than the mean-field result for smaller  $\kappa$ . Thus, the present density functional theory concepts with and without correlations in LDA complement each other. This approach allows to correctly reproduce the radially averaged properties of a Yukawa plasma in the (classical) ground state.

With the present approach the basis for a continuum theory of strongly correlated dusty plasmas has been laid. It is straightforward to extend this approach to finite temperatures as was shown by Wrighton *et al* [232]. In that case the density profile becomes smooth. It extends to larger distances and the abrupt density step is washed out. We underline that this theory yields only a part of the properties—the mean density profile and related average properties. The observed radial density modulation arising from the shell structure is, however, a correlation effect and is, thus, not reproduced by this approach. A theory which allows one to describe correlation effects will be discussed in section 7.2. Interestingly, the theoretical prediction of an inhomogeneous density profile in Yukawa balls could be verified experimentally by Block *et al* and co-workers [233, 234].

## 5. Dynamical properties

So far we have considered the zero temperature behavior of spatially confined dusty plasmas which is determined by the minima of the total potential energy. These minima correspond to either the ground state or metastable states of the cluster. Finite temperature will lead to excitations of the cluster—particles will oscillate around the local potential minima. Under normal experimental conditions, i.e. room temperature and strong coupling, the excitation energy is weak, and one can expand the total energy in a Taylor series around a stationary state to second order. This gives rise to the normal modes of the system which fully determine the dynamical and transport properties and are crucial for the melting behavior [213, 235] of strongly correlated finite systems at weak excitation. For these reasons, normal modes in classical trapped Coulomb systems have been extensively studied by many authors, (e.g. [213, 236–238]). Investigations

of Yukawa systems were reported in [210, 230, 239, 240], for other types of pair interactions in finite clusters, see e.g. [241–244].

### 5.1. Normal modes of finite systems

In the following we recall the main properties of normal modes of a  $d$ -dimensional finite system of  $N$  particles described by the general Hamiltonian (1), where  $U(\mathbf{r}) = U(|\mathbf{r}|)$ , and, at the end, apply the concept to harmonically confined dust crystals in two and three dimensions.

We start from the ground (or metastable) state of our system given by the  $d \times N$ -dimensional coordinate vector  $\mathbf{r}^* = (\mathbf{r}_1^*, \mathbf{r}_2^*, \dots, \mathbf{r}_N^*)$ , corresponding to a minimum of the total potential energy  $U_{\text{tot}}$  and thus fulfilling the equations ( $\sum'$  indicates the absence of terms with equal indices, and we denote  $\mathbf{r}_{il} = \mathbf{r}_i - \mathbf{r}_l$ )

$$\mathbf{0} = \nabla_i U_{\text{tot}}(\mathbf{r})|_{\mathbf{r}=\mathbf{r}^*} = \frac{U'(|\mathbf{r}_i^*|)}{|\mathbf{r}_i^*|} \mathbf{r}_i^* + \sum_{l=1}^N \frac{V'(|\mathbf{r}_{il}^*|)}{|\mathbf{r}_{il}^*|} \mathbf{r}_{il}^*,$$

$$\forall i \leq N. \quad (21)$$

Now consider an arbitrary small excitation,  $\hat{\mathbf{r}} = \mathbf{r} - \mathbf{r}^*$ , around this state for which a harmonic approximation of the potential can be applied

$$U_{\text{tot}}(\mathbf{r}) \approx U_{\text{tot}}(\mathbf{r}^*) + \frac{1}{2} (\mathbf{r} - \mathbf{r}^*)^T \mathcal{H}(\mathbf{r}^*) (\mathbf{r} - \mathbf{r}^*), \quad (22)$$

where equation (21) and the definition of the Hessian matrix  $\mathcal{H}(\mathbf{r}^*) = \nabla \nabla^T U_{\text{tot}}(\mathbf{r})|_{\mathbf{r}=\mathbf{r}^*}$  have been used. Since  $\mathcal{H}(\mathbf{r}^*)$  is a real, symmetric and positive semidefinite  $dN \times dN$  matrix, its eigenvalue problem

$$\lambda m \hat{\mathbf{r}} = \mathcal{H}(\mathbf{r}^*) \hat{\mathbf{r}}, \quad (23)$$

defines  $d \times N$  eigenvalues,  $\lambda_j \geq 0$ , and  $d \times N$  linearly independent eigenvectors  $\hat{\mathbf{r}}_j$ , which form a basis in the configuration space and are conveniently chosen to be orthonormal. Within this basis the excitation can be expanded,

$$\mathbf{r}(t) = \mathbf{r}^* + \sum_{j=1}^{dN} c_j(t) \hat{\mathbf{r}}_j, \quad (24)$$

so that the time dependence of an arbitrary excitation is fully determined by the coefficients  $c_j(t)$ —the *normal coordinates*. Using the equations of motion for particles described by the Hamiltonian (1) and equations (22)–(24), the equations for the normal coordinates follow

$$\mathbf{0} = m \ddot{\mathbf{r}} + \nabla U_{\text{tot}}(\mathbf{r}) \approx m \ddot{\mathbf{r}} + \mathcal{H}(\mathbf{r}^*) (\mathbf{r} - \mathbf{r}^*)$$

$$= m \sum_{j=1}^{dN} [\ddot{c}_j(t) + \lambda_j c_j(t)] \hat{\mathbf{r}}_j. \quad (25)$$

Due to the independence of the normal modes the solution is given by

$$c_j(t) = A_j \cos(\sqrt{\lambda_j} t + B_j), \quad \forall j \leq dN, \quad (26)$$

in which the constants  $A_j$  and  $B_j$  have to be determined from the initial conditions  $\mathbf{r}(0)$ ,  $\dot{\mathbf{r}}(0)$  of the excitation. The frequency of the normal mode  $j$  is given by the eigenvalue,

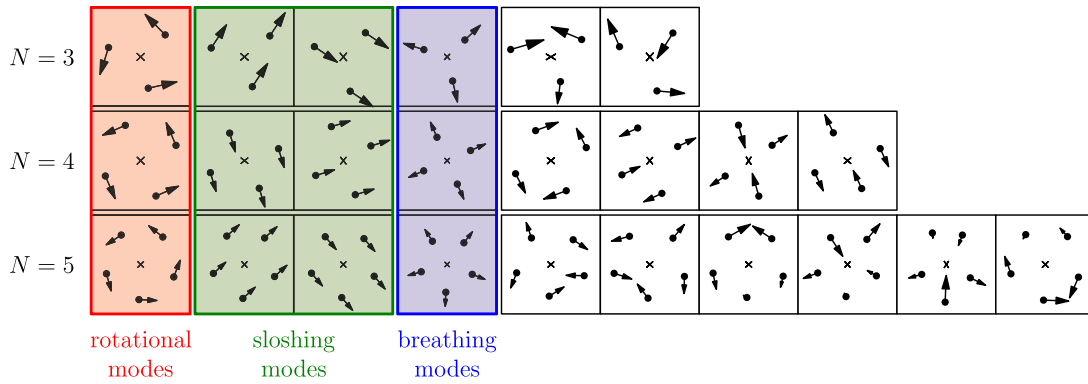


**Figure 15.** All normal modes of two-dimensional harmonically confined Coulomb systems with  $N = 3, 4, 5$  particles. The dots picture the particles within the ground state configuration, and the arrows show the direction and amplitude of the oscillatory motion. The  $N$ -independent modes, i.e. the rotational modes, the sloshing modes, and the breathing modes are highlighted. (Reprinted with permission from [248]. Copyright 2009 IOP Publishing.)

$\omega_j = \sqrt{\lambda_j}$  and the associated collective motion of all particles by the eigenvector  $\hat{r}_j$ .

With the normal modes the individual particle coordinates can be eliminated from all expressions. In particular, inserting expansion (24) into equation (1) diagonalizes the Hamiltonian which is thus transformed into a superposition of  $N \cdot d$  independent one-dimensional harmonic oscillators. This representation is very useful in order to obtain semi-analytical approximations for the transport and melting properties of strongly correlated systems, e.g. ([204, 213, 245]) and can also be extended to quantum systems, cf section 5.5. In the limit of a macroscopic system, the normal mode spectrum of a finite cluster approaches the phonon spectrum of an infinite crystal.

## 5.2. Normal modes of crystals in a spherical harmonic trap

**5.2.1. Coulomb systems.** For the investigation of the normal modes of harmonically confined Coulomb systems ( $\kappa = 0$ ) detailed theoretical studies have been performed for  $d = 1, 2, 3$  dimensions (see [213, 237, 238, 246, 247] and references therein). It was shown that there exist three (partially degenerate) normal modes, which are *universal*, i.e. they are independent of the particle number  $N$ , dimensionality  $d$  and configuration  $\mathbf{r}^*$ :

- (i) There are rotational modes ( $\lambda = 0$ ) corresponding to a rotation of the whole system which reflect the axial symmetries of the confinement potential.
- (ii) There are  $d$  sloshing modes (or Kohn modes [246],  $\lambda = \omega^2$ ) describing the oscillation of the system as a whole. The motion of the center of mass is independent of the interparticle forces.
- (iii) The breathing mode ( $\lambda = 3\omega^2$ ) describes a uniform radial expansion and contraction of all particles.

The existence of these three universal modes is illustrated for the two-dimensional systems with  $N = 3, 4, 5$  particles in figure 15, where all modes of these systems corresponding to the ground state configuration are shown.

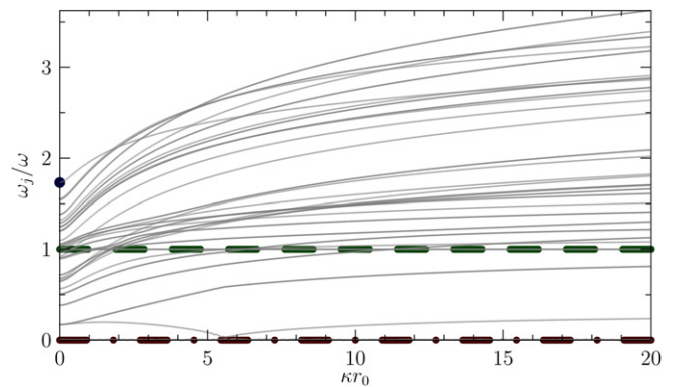


**Figure 16.** Screening dependence of the normal mode spectrum for a two-dimensional harmonically confined system of  $N = 16$  particles. The universal center of mass rotation (sloshing mode) is shown by the dashed–dotted (dashed) line, the uniform breathing mode exists in the Coulomb case only and is depicted by the dot at  $\kappa = 0$ . (Reprinted with permission from [248]. Copyright 2009 IOP Publishing.)

**5.2.2. Yukawa systems.** Since dusty plasmas exhibit a screened interaction between the particles the question arises how screening affects the normal mode spectrum of plasma crystals. Since the screening parameter  $\kappa$  enters the Hamiltonian (1) also the Hesse matrix  $\mathcal{H}$  and its eigenvalues will depend on  $\kappa$ . This dependence has been analyzed in detail by Henning *et al* [248]. An example of a 2D crystal with  $N = 16$  particles is shown in figure 16. The analysis shows that for Yukawa systems there are only two modes with a universal frequency: the center of mass oscillation and rotation, cf modes (i) and (ii) above. In contrast, the extension of the Coulomb breathing mode to finite  $\kappa$  values shows an increasing frequency which changes from  $\sqrt{3}\omega$ , for  $\kappa = 0$ , to  $\sqrt{5}\omega$ , for  $\kappa r_0 \gg 1$ . A simple analytical model for this frequency was developed by Sheridan [249, 250] which, however, assumes a constant mean density throughout the cluster which is justified only for weak screening, cf section 4.4.

## 5.3. Breathing mode versus monopole oscillation

The breathing mode—the radial and uniform collective expansion and contraction of all particles—is of special

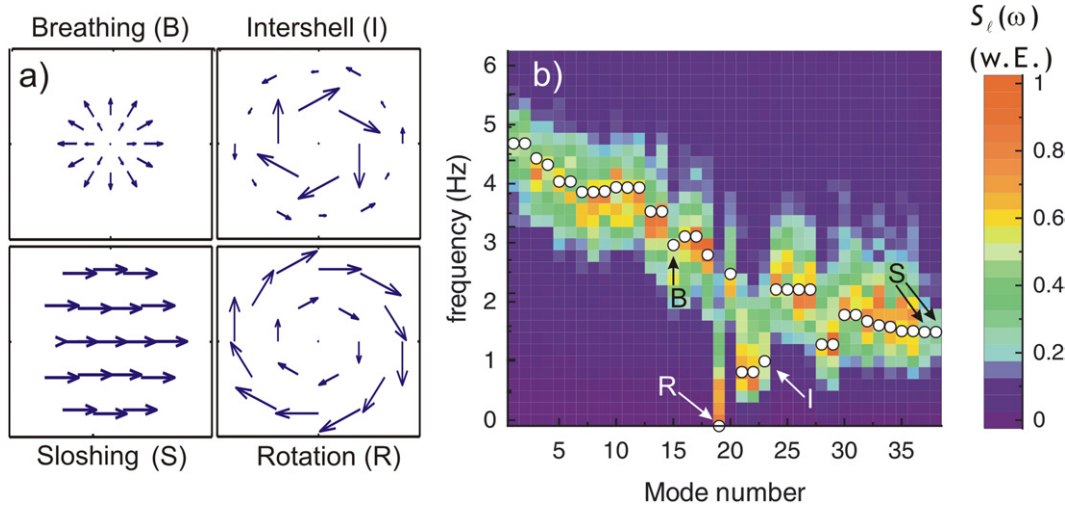


**Figure 17.** Experimental normal mode spectrum of a 2D dust cluster with  $N = 19$  particles. (a) Selected normal modes: breathing, sloshing, rotation of the whole cluster and inter-shell rotation. (b) Measured power density versus mode number. Arrows show the position of the four modes in (a). (Reprinted with permission from [264]. Copyright 2007 Deutschen Physikalischen Gesellschaft.)

relevance since it can be easily excited selectively by variation of the confinement [210] or by applying external fields [241]. In particular, the corresponding breathing frequency  $\omega_{\text{BM}}$  can often be precisely measured and may serve as a sensitive indicator of intrinsic system properties including the screening parameter and the particle charge in complex plasmas [210]. The continuum analog to the breathing mode is the *monopole oscillation* [237], which represents the lowest compressional mode within a hydrodynamic approach [251]. Due to the continuum character, this monopole oscillation is applicable to gas or fluid phases of classical [237, 250, 252] or quantum systems [253–255] where correlations are weak or moderate. In the strongly coupled crystalline state, however, where the particles become individually separated, the concept of the monopole oscillation is questionable. In order to use this concept also in the case of strong correlations, the monopole oscillation is often associated [210, 213, 256] with the oscillation of the mean square radius:

$$R^2(t) := N^{-1} \sum_{i=1}^N r_i(t)^2. \quad (27)$$

It was then shown [213, 237] that this oscillation is universal in 3D harmonically confined Coulomb systems, with a frequency,  $\omega_{\text{MO}} = \sqrt{3} \omega$ , equal to  $\omega_{\text{BM}}$ . A similar universal correspondence between  $\omega_{\text{MO}}$  and  $\omega_{\text{BM}}$  was observed for harmonically confined 2D systems if the interaction is a repulsive power law,  $\propto 1/r^n$  ( $n = 1, 2, \dots$ ), or logarithmic [256]. Due to this close connection some confusion of both concepts emerged [256]. Thus, the existence of a breathing mode is commonly assumed also for non-Coulomb systems, including Lennard-Jones clusters [238] or systems with Yukawa interaction [257–259]. We also mention a recent kinetic theory approach to the monopole oscillation [260].

However, while an oscillation of  $R^2$  can appear in all types of finite clusters, this is not the case for the breathing mode. The existence conditions of the uniform (i.e. self-similar with  $\hat{r}_i \sim r_i^*$ , for all particles) breathing mode have recently been

derived by Henning *et al* [261] and can be summarized as follows. A configuration- and  $N$ -independent, breathing mode exists:

- in the case of a harmonic confinement,  $U(r) = m\omega^2 r^2/2$ , with particles interacting via potentials  $V(r)$  proportional to  $1/r^\gamma$  or to  $\log(r)$ . In these cases the breathing frequency is generally given by  $\omega_{\text{BM}} = \sqrt{2 + \gamma} \omega$ ,
- for interaction potentials proportional to  $r^2$  if the confinement has the form  $r^2 \log(r)$ . In this case also the prefactor of the confinement determines the breathing frequency,
- in the case of stationary states with a special symmetry, for example platonic bodies, a uniform breathing mode exists for any pair interaction. This is restricted to small clusters typically having only a single shell.

These results are valid for any real  $\gamma$  and any dimension and coincide, in special cases, with the results of the monopole oscillation [256]. Furthermore, the conclusion follows that no universal breathing mode exists for exponential interaction potentials (such as Yukawa and Morse) or non-monotonic ones (e.g. Lennard-Jones). Interestingly, as a consequence, these systems possess multiple monopole modes.

#### 5.4. Normal modes in dusty plasma experiments

A remarkable feature of dusty plasmas is that the normal modes are directly accessible in experiments. Melzer has performed detailed measurements of the normal mode spectrum of small 1D and 2D dust crystals [210, 262] (for an overview see [263]). In one type of experiments the thermally excited particles were traced and the associated power spectrum was recorded. In other experiments, certain normal modes were selectively excited by focusing a laser beam on selected particles, including rotation of the whole cluster and inter-shell rotations. Examples are shown in figure 17. Recently, first measurements of the normal mode spectrum of 3D Yukawa balls have been reported [248, 265]. An example of a Yukawa

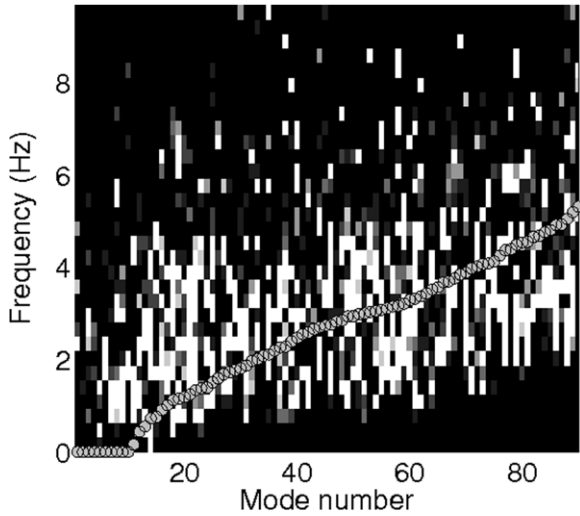


**Figure 18.** Experimental normal mode spectrum of a Yukawa ball with  $N = 31$  particles. The spectral power density is shown in gray-scale with brighter colors corresponding to higher power. Gray dots show the best fit to the theoretical power density computed from the normal modes. (Reprinted with permission from [265]. Copyright 2009 American Physical Society.)

ball with 31 particles is shown in figure 18 displaying the measured frequencies of all 93 normal modes compared with the theoretical predictions.

For a quantitative comparison of the experimental results with theory it is important to take into account dissipation effects which are missing in the discussion of section 5.1. This is straightforward and has recently been performed in [248, 266]. Dissipation has a substantial effect on the spectral properties: it leads to a broadening of the spectral peaks and to a red shift and, ultimately, to a disappearance of low frequency modes from the spectra.

### 5.5. Normal modes of strongly correlated quantum systems

The concept of normal modes is very useful for strongly correlated quantum systems as well. In terms of the normal modes the Hamilton operator can be diagonalized and used to obtain an analytical solution for the  $N$ -particle wave function which is a simple superposition of  $d \cdot N$  harmonic oscillator wave functions. This has been demonstrated for electrons in quantum dots and indirect excitons in coupled quantum dots by Balzer *et al* (cf [267, 268] and references therein).

A variety of normal modes of confined quantum systems have been studied in some detail for electrons in quantum dots and for ultracold atomic gases in traps. In particular, the sloshing (Kohn) mode was analyzed, including the extension to the case of a magnetic field [246, 247]. The independence of this mode of the interaction between the particles is also an important consistency test for approximate theories and simulations [269]. Besides the Kohn mode, the breathing mode (more precisely, the monopole mode, cf. section 5.3) also has been intensively studied [254, 270]. Its dependence on the type of the interaction potential was investigated by several authors, including  $1/r^2$  potentials [270] and dipole interaction [271]. A detailed study of the breathing frequency in the whole

range of coupling strengths, from the ideal quantum system to the strongly coupled crystal-like state, has recently been performed by Bauch *et al* [254]. They found that, in contrast to classical systems, quantum systems possess two breathing modes one of which is associated with the center of mass motion and has a universal frequency of  $2\omega$ . They also reported an interesting dependence of the standard breathing frequency on the system dimensionality and on the spin statistics. These dependences are of interest for experiments with trapped atomic gases and for electrons or excitons in quantum dots and may develop into a sensitive diagnostics just as it has been demonstrated for dusty plasmas.

## 6. Thermodynamics and phase transitions

When the plasma crystal is heated particles start to oscillate in their local potential minima. At sufficiently strong heating these fluctuations become overcritical and the crystal melts. Melting and freezing are well studied in macroscopic systems and they can be characterized by many quantities. One is the coupling parameter which has a critical value  $\Gamma_M$  at the melting point. Alternatively melting can be diagnosed from order parameters, the shape of the pair distribution function (the ratio of maxima and minima falls under a critical value) or the static structure factor (e.g. [272]). Other sensitive quantities are the specific heat  $C_v$  or the total energy autocorrelation function [273] (the indices  $i$  and  $k$  denote either a time argument or a Monte Carlo step in a thermodynamic simulation)

$$C_E(k) = \frac{\sum_{i=1}^{L-k} (E_{i+k} - \langle E \rangle) (E_i - \langle E \rangle)}{(L-k) (\langle E^2 \rangle - \langle E \rangle^2)}, \quad (28)$$

which will be discussed below. Finally, an important quantity is the magnitude of the particle position fluctuations around the equilibrium position,

$$u_L^2 = \frac{1}{N} \sum_{i=1}^N \langle (r_i - r_i^0)^2 \rangle, \quad (29)$$

originally discussed by Lindemann [274]. But when applied to two-dimensional systems,  $u_L^2$  shows a logarithmic divergence with system size according to the Landau–Peierls theorem (e.g. [275]), and also the displacement autocorrelation function diverges [276]. This led to modified quantities, including the *relative interparticle distance fluctuations* (IDF) [277–279]

$$u_{\text{rel}} = \frac{2}{N(N-1)} \sum_{1 \leq i < j} \sqrt{\frac{\langle r_{ij}^2 \rangle}{\langle r_{ij} \rangle^2}} - 1, \quad (30)$$

which are well behaved in low dimensional systems. Below we will consider melting of finite Coulomb crystals. Readers interested in general aspects of melting and the analysis with computer simulations are referred to the dedicated reviews by Löwen [280] and Hartmann *et al* [272]. The peculiarities of melting in two-dimensional systems related to the Kosterlitz–Thouless scenario [281, 282] have also been studied in dusty plasmas (e.g. [283]).

### 6.1. Melting in finite systems

A phase transition is a phenomenon observed in macroscopic systems for which the thermodynamic limit can be applied. Therefore, in finite systems such as plasma crystals in traps, the notion of a phase transition such as melting requires a special analysis. It has been observed in many finite systems, including electrons in quantum dots [284, 285] or clusters [279] that upon heating the collective particle behavior changes from solid-like to liquid-like. Instead of a ‘true’ phase transition a crossover is observed which extends over a finite range of temperatures (of the order parameter), cf. figures 19(b). This makes the definition of a ‘melting point’ ambiguous, moreover, various quantities including the specific heat, the energy correlation function (28) or the distance fluctuations (30) need not necessarily agree with their predictions of the melting point. Some examples are shown in the right column of figure 19.

These difficulties have their physical origin in finite size effects. Melting can occur via several mechanisms such as excitation, coupling or softening of certain normal modes, via creation of defects or oscillation between stationary states (e.g. [286, 287]). Böning *et al* have discussed a simple example which is very intuitive [273]. They considered a 2D ‘cluster’ of just four particles in a spherical confinement. This system has a single stationary state where the particles are located at the corners of a square of side length  $a$ . An increase in temperature (lowering of  $\Gamma$ ) has two effects. Firstly, particles start to oscillate around their ground state positions (in the local potential minima). Secondly, two particles can exchange their positions. This is a rare event since it requires to overcome a certain potential barrier and requires a coordinated motion of (at least) two particles. This coexistence of local fluctuations and hopping events changes when the temperature is increased and shows similarities with a melting process. This is shown in the left column of figure 19 where the time-dependent fluctuating distance of a pair of particles with a mean distance  $b = \sqrt{2}a$  is shown. In the ‘solid-like’ state close to the ground state, hopping events are exponentially rare. An increase in temperature leads to a growing frequency of these events during which the distance changes from  $a$  to  $b$  and vice versa, and in the ‘liquid-like’ state hopping events occur constantly.

This behavior is not adequately captured by the distance fluctuations  $u_{\text{rel}}$ , equation (30), although the general trend of an increase with  $T$  is seen, cf figure 19(b). Even worse, the behavior of  $u_{\text{rel}}$  as a function of  $T$  depends on the way it is computed [273]. When the simulation length is increased the increase in  $u_{\text{rel}}$  shifts to lower and lower temperatures because the probability of capturing a hopping event is increased. A solution to this dilemma consists of recording not just the mean value of the distance fluctuations but the whole probability distribution of distance fluctuations  $P(u_{\text{rel}})$ . This function has a peak around small values of  $u_{\text{rel}}$  associated with local fluctuations which are dominant in the ‘solid’ state. In contrast, in the ‘liquid’ state there is a peak around a larger value of  $u_{\text{rel}}$  associated with the hopping events. In the transition region, in the vicinity of the ‘melting’ point,  $P(u_{\text{rel}})$  has a large width (in some cases there are two peaks, see figure 21). This behavior is well captured by the second moment of the fluctuations,  $\sigma_{u_{\text{rel}}}$ ,

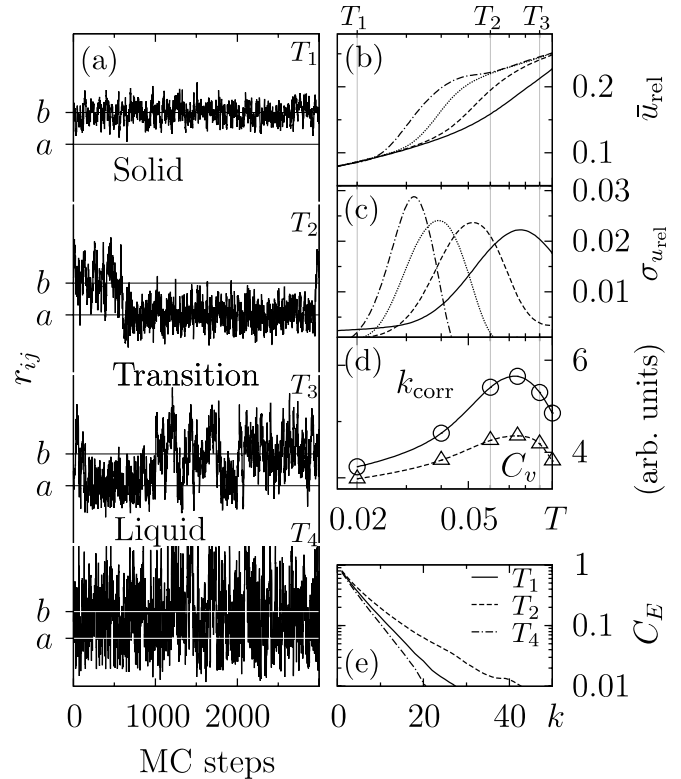


**Figure 19.** (a) Distance of an arbitrary pair of  $N = 4$  classical particles in 2D as a function of Monte Carlo step. From top to bottom:  $T_1 = 0.02$  (solid-like),  $T_2 = 0.06$  and  $T_3 = 0.09$  (transition region), and  $T_4 = 0.5$  (liquid-like).  $a$  and  $b = \sqrt{2}a$  denote the two possible interparticle distances in the ground state. (b) Temperature dependence of the mean block averaged IDF  $\bar{u}_{\text{rel}}$ , for different block lengths  $M = 10^3, 10^4, 10^5, 10^6$  (right to left) (equivalent to computing  $u_{\text{rel}}$ , equation (30), from multiple simulations of length  $L = M$ ). (c) The corresponding second moment  $\sigma_{u_{\text{rel}}}$ , equation (31). (d) Specific heat  $C_v$  and energy correlation time  $k_{\text{corr}}$ . (e) Total energy autocorrelation function  $C_E$ , equation (28), for three of the temperatures in (a). (Reprinted with permission from [273]. Copyright 2008 American Physical Society.)

i.e. the variance of the block averaged interparticle distance fluctuations (VIDF) [273]:

$$\sigma_{u_{\text{rel}}} = \sqrt{\frac{1}{K} \sum_{s=1}^K u_{\text{rel}}^2(s) - \langle u_{\text{rel}} \rangle^2}, \quad \langle u_{\text{rel}} \rangle = \frac{1}{K} \sum_{s=1}^K u_{\text{rel}}(s). \quad (31)$$

This allows one to obtain a reasonable estimate of the melting temperature  $T_M$  from the peak of  $\sigma_{u_{\text{rel}}}(T)$ . In equation (31) the whole simulation duration  $L$  was split into  $K$  equal blocks of length  $M$ , i.e.  $L = K \cdot M$ , and  $u_{\text{rel}}$  is computed for each block  $s$  with a subsequent average over all blocks. In this approach the ‘proper’ value of  $M$  remains open, and the authors used the maximum of the energy correlation time,  $k_{\text{corr}}(T) = \sum_k C_E(k, T)$ , cf figure 19(d), which is sensitive to melting, to fix the value of  $M$ .

### 6.2. Melting of Yukawa balls: experiment and simulation

The dynamical behavior of small trapped systems has been studied in a number of recent experiments with Yukawa balls

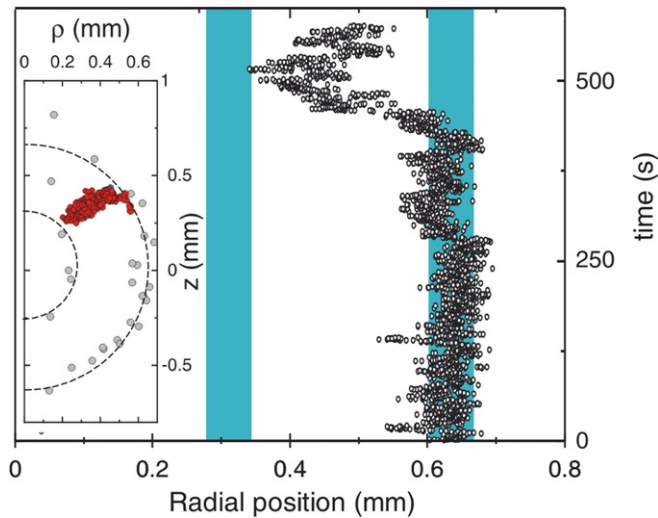


**Figure 20.** Experimentally observed inter-shell transition in a small Yukawa ball with  $N = 31$  particles. (Left) Particle positions (gray) and trace of one particle moving from the outer shell inward and back (red) in the  $\rho$ - $z$  plane. (Right) Time-resolved radial component of the trajectory of the particle leaving the outer shell. Vertical (blue) stripes indicate the location of the two shells. (Color online.)

[233, 234]. In particular, transitions of particles between shells or, in other words, transitions of Yukawa balls between two different stationary states could be followed in detail. An example of a cluster of 31 particles is shown in figure 20. There, the dynamics of one particle is recorded as a function of time. The particle first oscillates in its local potential minimum for about 400 s and then undergoes a ‘hopping’ event as discussed above: it moves from the outer shell to the inner shell and rapidly returns to the outer shell. Thereby the cluster state, for a short period of time of about 50 s, changes from the ground state (4, 27) to the excited state (5, 26). The reason for this rapid return can be traced to the local potential landscape—the potential barrier from state (5, 26) to (4, 27) is much lower than vice versa [288]. This shows that dusty plasma experiments allow one to directly probe the total potential landscape of strongly correlated plasmas.

The concepts for melting in finite systems developed above can be directly applied in computer simulations of Yukawa balls. An example of Monte Carlo simulations is presented in figure 21. There for a crystal of 40 particles the mean distance fluctuations (30), the variance of the distance fluctuations (31) and the probability distribution  $P(u_{\text{rel}})$  are shown. As discussed in section 6.1 the distance fluctuations  $u_{\text{rel}}$  increase very gradually with temperature; however, their variance shows a distinct peak around the melting point. Also, the distance fluctuations and their probability distribution (right part of figure 21) exhibit the characteristic broadening and indications of a two-peak structure in the vicinity of the melting temperature discussed above.

In recent years there have been numerous theoretical studies of melting in spherical plasma crystals. Golubnychiy *et al* have shown that the melting temperature of small clusters varies non-monotonically with the cluster size [289]. It closely follows the stability of the clusters, cf section 4.3: particularly high ‘melting’ temperatures were observed for

$N = 6, 12, 13$  all of which are stable with high values of the mean Voronoi symmetry parameter (equation (12)). Apolinario *et al* investigated larger two-dimensional and three-dimensional clusters in anisotropic confinements and observed inhomogeneous melting and the existence of several melting transitions where first the order within a shell is lost, followed by a decoupling of different shells, at a higher temperature [235, 287]. Finally, the melting temperature of large Coulomb balls was studied in detail by Schiffer [290] who found that it is generally lower than in a macroscopic crystal and investigated the transition to this limit.

Thus, summarizing this section, we have shown that the concept of phase transitions can be extended to finite systems and the melting point is reasonably well estimated by the specific heat, the maximum of the energy autocorrelation function or the VIDF, equation (31). Dusty plasmas are well suited to test these concepts by direct measurements. Here systematic experimental studies in a broad range of parameters are still missing and are expected to become possible in the near future. Finally, we note that the concept of ‘melting’ in application to small systems should be of relevance also in other fields of strongly correlated systems. In particular it was shown that the presented melting criterion based on the VIDF is applicable not only to small classical clusters but also to finite quantum crystals [273].

## 7. Liquid behavior

Complex plasmas are perfectly suited to study thermodynamic and transport properties in strongly correlated systems, in particular in the liquid state. One can measure not only macroscopic properties as e.g. in conventional fluids, but it is possible to perform measurements even by tracking individual particles. As an example we briefly discuss the recent observation of anomalous diffusion in two-dimensional plasma layers.

### 7.1. Anomalous diffusion

Stimulated by theoretical predictions [291] that in purely 2D systems diffusion should deviate from the Einstein formula for the particle displacements

$$u(t) = \langle |\mathbf{r}(t) - \mathbf{r}(t_0)|^2 \rangle = t^\alpha, \quad \text{with } \alpha = 1, \quad (32)$$

where the averaging is performed over all particles, a series of experiments has recently been performed [187, 190, 191, 292–298]. As an example, we show in figure 22 the results of Liu *et al*, for the friction and screening parameters  $\nu = 0.2$  and  $\kappa = 0.9$ , clearly indicating values of  $\alpha > 1$ , so-called ‘superdiffusion’. The measurements were complemented by first-principle computer simulations [189, 297, 299–303]. The majority of these works predicted significant deviations from normal diffusion, mostly toward  $\alpha > 1$ , although a large scatter of  $\alpha$ -values from one to 1.3 was reported.

The systematic analysis of Ott *et al* indicates [301] that superdiffusion reaches a maximum in the strongly coupled liquid state at a temperature about 5 times higher than the melting point,  $T \approx 5T_m$ , corresponding to  $\Gamma \approx 0.2\Gamma_M$ , cf left

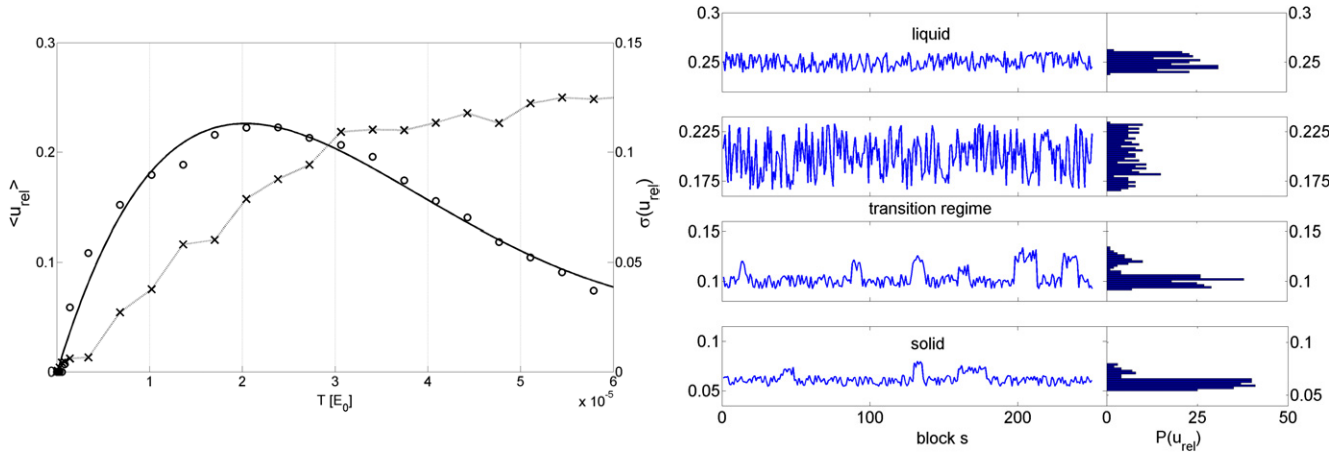


**Figure 21.** (Left) Mean distance fluctuations (equation (30), crosses) and their variance (equation (31), circles), versus temperature around the melting point  $T_M$ , for a Yukawa ball with  $N = 40$  and  $\kappa = 0.4$ . (Right) Block averaged interparticle distance fluctuations  $u_{\text{rel}}(s)$  versus block number  $s$  during a Monte Carlo simulation and their accumulated probability  $P$  (rightmost column) for four temperatures (from bottom to top): below, close to, at and above  $T_M$ . Block length  $M = 1000$ . (Reprinted with permission from [288]. Copyright 2009 Wiley-VCH Verlag.)

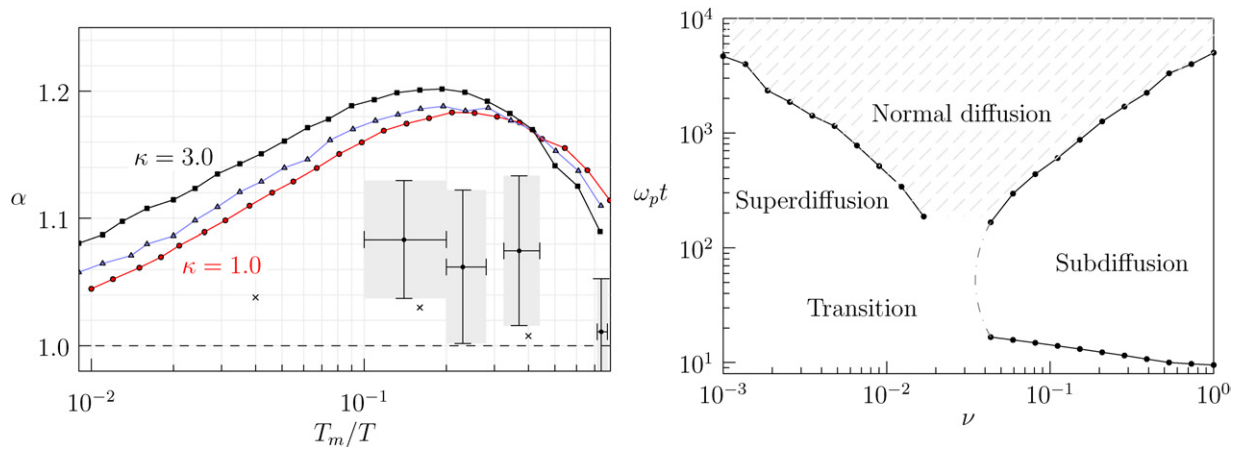


**Figure 22.** (Left) Experimental and simulation results for the diffusion exponent in a 2D Yukawa plasma as a function of inverse temperature (normalized to the melting temperature). Lines are Langevin simulations for  $\kappa = 1.0, 2.0, 3.0$  and no dissipation,  $\nu = 0$ . Three small crosses indicate results with a dissipation of  $\nu = 0.02$  and  $\kappa = 3$ . Experimental data for  $\kappa = 0.90$  and  $\nu = 0.02$  from Liu *et al* [296] are indicated by the gray boxes with error bars in the lower right and are averaged over temperature regions, as indicated, and correspond to  $T_m \approx 6000$  K. (Right) Diffusion regimes observed in the simulations for  $\Gamma = 200$  and  $\kappa = 3$  as a function of time for different dissipation parameters  $\nu$  in units of  $\omega_p$ . (Figure courtesy of T Ott.) (Color online.)

part of figure 22. This trend is easy to understand: when the coupling is reduced, superdiffusion gradually vanishes since excitation of collective modes requires sufficiently strong interaction between the particles. On the other hand, at very strong coupling, particles are increasingly localized in the minima of the total potential energy (these ‘caging’ effects have been investigated in detail by Donko *et al* [304, 305]) and the system approaches the crystallization point  $\Gamma_M$ . As a consequence, particle mobility is reduced again resulting in normal diffusion and, ultimately, subdiffusion. The physical origin of the collective modes responsible for superdiffusion is still open and more recent substantially longer simulations with a larger particle number indicate that superdiffusion is only a transient phenomenon, see the right part of figure 22. This is particularly clear in a dissipative system, and the figure shows the results for a broad range of friction coefficients  $\nu$  (in units of plasma frequency). After sufficiently long times

of about  $10^3$ – $10^4$  plasma cycles the system apparently returns to normal diffusion, for dissipative and even for friction-less systems [306, 307].

The experimental results in figure 22 are substantially below the simulation data obtained without dissipation (lines). If dissipation is included at a level as expected in the experiment (cf three data points marked by the small crosses) the data fall below the experiment. It is clear that the qualitative trends are captured by the simulations; however, quantitative discrepancies remain. They are, most likely due to different time scales during which the diffusion exponent has been extracted. As the right part of figure 22 shows, this has crucial effect on the value of  $\alpha$ . More precise comparisons and resolution of these questions should be possible in the near future. The behavior of the diffusion coefficient is expected to be typical for the transport properties of strongly correlated

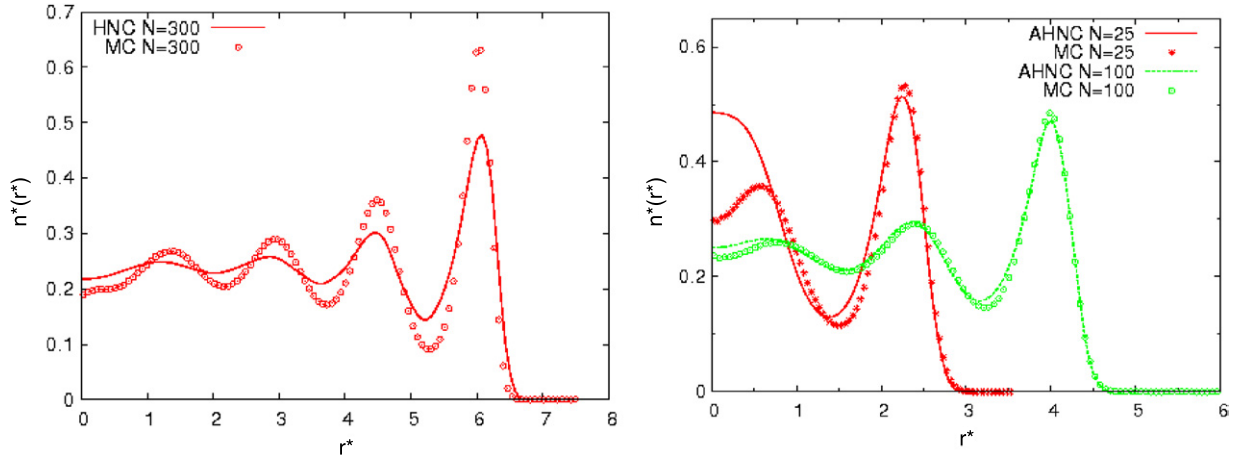


**Figure 23.** Radial density profile of Coulomb balls ( $\kappa = 0$ ) with  $N = 25, 100, 300$  particles in the liquid phase. Symbols denote Monte Carlo simulations and lines standard HNC and the improved HNC (AHNC). In the right (left) figure  $\Gamma = 20$  ( $\Gamma = 40$ ). (Reprinted with permission from [309]. Copyright 2009 American Physical Society.)

plasmas. It clearly shows the important role of collective effects. Still many of these effects are not yet fully explored.

### 7.2. Theoretical description of strong correlations in the fluid state

In section 4.4 we have presented an analytical approach to strongly correlated confined plasmas which was based on a classical version of density functional theory. The results in mean-field approximation and in local density approximation were shown to well reproduce the spatially averaged properties of the Coulomb and Yukawa balls, in particular the mean density profile. However, the typical trends of particle localization in shells, which are observed in simulations and in the experiments in the strong coupling regime, were missed by these approximations. An extension of this approach both to finite temperatures and to the strongly coupled liquid regime was recently developed in a series of papers by Kraeft *et al* [308] and Wrighton *et al* [232, 309, 310]. The basis is the classical theory of liquids. The external potential  $U$  induces a non-uniform equilibrium density  $n(r)$ . It follows from density functional theory that  $n(r)$  obeys the equation [311]

$$\ln \frac{n(r)\Lambda^3}{z} = -\beta U(r) - \beta \frac{\delta F_{\text{ex}}(\beta | n)}{\delta n(r)}, \quad (33)$$

where  $z = e^{\beta\mu}$ ,  $\mu$  is the chemical potential and  $\Lambda = (h^2\beta/2\pi m)^{1/2}$  is the thermal de Broglie wavelength. The excess free energy  $F_{\text{ex}}(\beta | n)$  is a universal functional of the density for the Hamiltonian (1), independent of the applied external potential  $U$ , and describes all correlations among the particles. The solutions to (33) are such that there is a unique equilibrium density  $n(r)$  for each  $U(r)$ , using the same  $F_{\text{ex}}(\beta | n)$ .

Equation (33) can be transformed by introducing the direct correlation function of the uniform OCP,  $c$ , evaluated at the average trap density  $\bar{n} = 3m\omega^2/(4\pi Q^2)$  [309]:

$$\ln \frac{n(r)\Lambda^3}{z} = -\Gamma \frac{1}{2} r^{*2} + \int d\mathbf{r}' n^*(r') c(|\mathbf{r}^* - \mathbf{r}'^*|; \Gamma) - \Gamma B(r^* | n^*), \quad (34)$$

where the function  $B(r | n)$  is referred to as bridge function for the trapped system. Here, correlations are introduced via the direct correlation function and the bridge function. The mean-field results of section 4.4, generalized to finite temperature, follow by neglecting correlations, i.e. setting  $B \rightarrow 0$  and  $c(r) \rightarrow -\Gamma/r$ .

To go beyond the mean-field limit, the authors of [309] considered two approximations: the HNC approximation and an augmented version of the HNC (AHNC). The HNC approximation follows by neglecting, as before, the bridge terms,  $B \rightarrow 0$  and computing the direct correlation function from the Ornstein–Zernicke equation (35) with the HNC closure relation (36), where  $g(r)$  denotes the pair distribution,

$$g(r) - 1 = c(r) + \int d\mathbf{r}' \{g(r') - 1\} c(|\mathbf{r} - \mathbf{r}'|; \Gamma), \quad (35)$$

$$\ln g(r) = -\frac{\Gamma}{r} + \int d\mathbf{r}' \{g(r') - 1\} c(|\mathbf{r} - \mathbf{r}'|; \Gamma). \quad (36)$$

Equations (35) and (36) are a closed set of equations to determine  $g(r)$  and  $c(r)$  for the OCP [3] which is here generalized to strongly correlated trapped systems by means of equation (34).

The results of the solution of the closed system (34)–(36) for a system for 300 charged particles with Coulomb interaction in a trap are shown in the left part of figure 23. The curves correspond to a strongly correlated liquid state at  $\Gamma = 40$  and are compared with exact results from Monte Carlo simulations [309]. In contrast to the mean-field approximation, the HNC result indeed reproduces the formation of shells. Overall there is a good qualitative agreement with the simulations: the number of shells and their positions are correctly reproduced. However, there are some quantitative discrepancies: the height of the peaks is underestimated by about 30%, and the width of the shells is too large.

The origin of these errors is, of course, the neglect of the bridge diagrams. Interestingly, these discrepancies could be almost completely removed by a simple choice of the bridge functions [309, 312]  $B(r|n) = \lambda(\Gamma)U(r)$ . The

results of this improved scheme (AHNC) with the choice  $\lambda = 0.6$  are included in the right part of figure 23. There two cases of  $N = 25, 100$  for  $\Gamma = 40$  are shown and reveal a surprising agreement with the simulations. Now even the width and height of the density peaks are reproduced within about 2%. This shows that the present augmented HNC model adequately describes the thermodynamic properties of the strongly coupled liquid state of trapped charged particles. An extension to even larger couplings with  $\Gamma \leq 100$  has been presented in [310] indicating that even a description of the crystal state should be possible.

Finally, we mention another interesting theoretical approach to strongly correlated plasmas—the quasi-localized charge approximation due to Kalman and Golden [313, 314] which has proved to be efficient to compute the dielectric and spectral properties of strongly correlated dusty plasmas, such as the dust acoustic wave [315].

## 8. Conclusions

In this paper an overview of strongly correlated dusty plasmas has been given. We started with a brief summary of the historical developments—from the first predictions of the plasma crystal by Ikezi and the first experimental realization and proceeded to very recent results in this very active field. We presented a diverse collection of experimental results and figures which demonstrate the unique opportunities provided by dusty plasmas: due to the large particle size and associated large charge strong correlation effects are achieved at room temperature, millimeter length scales and second time scales. This allows one to directly view and record the position and the motion of individual particles and to study many-particle properties both in large and finite systems with a precise particle number at the smallest (kinetic) level with maximum ('atomic') resolution. Thus, dusty plasmas are indeed an ideal 'laboratory' for strong correlation effects. Since under conditions of strong coupling many universalities are observed which are caused by the interaction, it is expected that many of the results from dusty plasmas will be of (at least qualitative) relevance also for other strongly correlated systems, including quantum gases in traps and optical lattices, ions and ultracold neutral plasmas in traps, electrons in quantum dots or the quark–gluon plasmas.

Our main goal was to highlight some of the most remarkable strong correlation effects observed in dusty plasmas: formation of crystalline structures, coexistence of ground and metastable states, collective excitations (normal modes) and solid–liquid phase transitions. These effects were discussed on the example of finite dust clusters in close comparison of experiments, theory and simulation. Naturally, this review had to omit many exciting experimental and theoretical results. Among the questions not covered are the effect of impurities and of non-spherical particles on the crystal structure. Further interesting topics are dusty plasmas in external electric and magnetic fields where first results show that the interaction potential between dust particles can be externally controlled [316], very similar to semiconductors (e.g. [317]). Furthermore, there have been recent results on

the non-equilibrium dynamics and short-time behavior of dusty plasmas (e.g. [245, 266, 318, 319]). Among the exciting topics of current research are phenomena at the shortest time scales, including the formation of binary correlations, anomalous transport (in analogy to superdiffusion), non-Newtonian viscosity [320], non-reciprocal forces due to streaming ions and electrons and magnetized dusty plasmas.

## Acknowledgments

The authors gratefully acknowledge many fruitful discussions and comments from our colleagues J W Dufty, H Kählert, P Ludwig, A Melzer, T Ott and A Piel. They thank H Baumgartner, H Kählert, P Ludwig, A Melzer and T Ott for contributing figures to this paper. This work is supported by the Deutsche Forschungsgemeinschaft via SFB-TR 24 grants A3, A5 and A7.

## References

- [1] Bonitz M 1998 *Quantum Kinetic Theory* (Leipzig: Teubner)
- [2] Falkenhagen H 1971 *Theorie der Elektrolyte* (Leipzig: Hirzel Verlag)
- [3] Hansen J P and McDonald I 2006 *Theory of Simple Liquids* 3rd edn (New York: Academic)
- [4] Debye P and Hückel E 1923 *Phys. Z.* **24** 185
- [5] Planck M 1888 *Wied. Ann.* **34** 139
- [6] Arrhenius S 1887 *Z. Phys. Chem.* **1** 631
- [7] Bjerrum N 1926 *K. Dan. Vidensk. Selsk. Mat.-Fys. Medd.* **VII** 9 1
- [8] Bogolyubov N 1962 *Problems of a Dynamical Theory in Statistical Physics* (Amsterdam: North-Holland) (Russian edition 1946)
- [9] Boroudjerdi H, Kim Y W, Naji A, Netz R, Schlagberger X and Serr A 2005 *Phys. Rep.* **416** 129–99
- [10] Löwen H 2008 *J. Phys.: Condens. Matter* **20** 404201
- [11] Imada M, Fujimori A and Tokura Y 1998 *Rev. Mod. Phys.* **70** 1039
- [12] Essler F H L, Frahm H, Göhmann F, Klümper A and Korepin V E 2005 *The One-Dimensional Hubbard Model* (Cambridge: Cambridge University Press)
- [13] Anzai S and Ozawa K 1968 *J. Phys. Soc. Japan* **24** 271–4
- [14] Sparks J T and Komoto T 1968 *Rev. Mod. Phys.* **40** 752
- [15] Anzai S, Matoba M, Hatori M and Sakamoto H 1986 *J. Phys. Soc. Japan* **55** 2531–4
- [16] McMahan A, Huscroft C, Scalettar R and Pollock E 1998 *J. Comput.-Aided Mater. Des.* **5** 131–62
- [17] Wolfe R, Wernick J H and Haszko S E 1965 *Phys. Lett.* **19** 449–50
- [18] Ramirez A P 1997 *J. Phys.: Condens. Matter* **9** 8171–99
- [19] Kotliar G and Vollhardt D 2004 *Phys. Today* **57** 53
- [20] Köhl M, Moritz H, Stöferle T, Günter K and Esslinger T 2005 *Phys. Rev. Lett.* **94** 080403
- [21] Greiner M, Mandel O, Esslinger T, Hänsch T W and Bloch I 2002 *Nature* **415** 39–44
- [22] Köhler T, Góral K and Julienne P S 2006 *Rev. Mod. Phys.* **78** 1311–51
- [23] Ohashi Y and Griffin A 2002 *Phys. Rev. Lett.* **89** 130402
- [24] Chen Q, Stajic J, Tan S and Levin K 2005 *Phys. Rep.* **412** 1–88
- [25] Phillips W D 1998 *Rev. Mod. Phys.* **70** 721
- [26] Bloch I, Dalibard J and Zwerger W 2008 *Rev. Mod. Phys.* **80** 885–80
- [27] Adams J *et al* 2005 *Nucl. Phys. A* **757** 102–83
- [28] Adcox K *et al* 2005 *Nucl. Phys. A* **757** 184–283

- [29] Back B et al 2005 *Nucl. Phys. A* **757** 28–101
- [30] Arsene I et al 2005 *Nucl. Phys. A* **757** 1–27
- [31] Gazdzicki M 1999 *Acta Phys. Pol. B* **30** 3611–20
- [32] NA50 Collaboration 2000 *Phys. Lett. B* **477** 28–36
- [33] Collaboration A 2008 *J. Instrum.* **3** S08002
- [34] Collins J C and Perry M J 1975 *Phys. Rev. Lett.* **34** 1353
- [35] Shuryak E V 1978 *Z. Eksp. Teor. Fiz.* **74** 408–420
- [36] Heinz U 2009 *J. Phys. A: Math. Theor.* **42** 214003
- [37] Müller B and Nagle J L 2006 *Annu. Rev. Nucl. Part. Sci.* **56** 93–135
- [38] Peshier A, Kämpfer B and Soff G 2002 *Phys. Rev. D* **66** 094003
- [39] Shuryak E 2004 *J. Phys. G: Nucl. Part. Phys.* **30** S1221–4
- [40] Hofmann M, Bleicher M, Scherer S, Neise L, Stöcker H and Greiner W 2000 *Phys. Lett. B* **478** 161–71
- [41] Gelman B A, Shuryak E V and Zahed I 2006 *Phys. Rev. C* **74** 044909
- [42] Gelman B A, Shuryak E V and Zahed I 2006 *Phys. Rev. C* **74** 044908
- [43] Filinov V, Bonitz M, Ivanov Y, Skokov V, Levashov P and Fortov V 2009 *Contrib. Plasma Phys.* **49** 536–43
- [44] Thoma M 2004 *IEEE Trans. Plasma Sci.* **32** 738–41
- [45] Thoma M H 2005 *J. Phys. G: Nucl. Part. Phys.* **31** L7–L12
- [46] Wineland D J, Bergquist J C, Itano W M, Bollinger J J and Manney C H 1987 *Phys. Rev. Lett.* **59** 2935
- [47] Drewsen M, Jensen I, Lindballe J, Nissen N, Martinussen R, Mortensen A, Staunum P and Voigt D 2003 *Int. J. Mass Spectrom.* **229** 83–91
- [48] Saiz E G et al 2008 *Nature Phys.* **4** 940–44
- [49] Ernstorfer R, Harb M, Hebeisen C T, Sciaini G, Dartigalongue T and Miller R J D 2009 *Science* **323** 1033–7
- [50] Killian T C, Kulin S, Bergeson S D, Orozco L A, Orzel C and Rolston S L 1999 *Phys. Rev. Lett.* **83** 4776–9
- [51] Pohl T, Pattard T and Rost J M 2004 *Phys. Rev. Lett.* **92** 155003
- [52] Rolston S L 2008 *Physics* **1** 2
- [53] Killian T C, Pattard T, Pohl T and Rost J 2007 *Phys. Rep.* **449** 77
- [54] Bonitz M et al 2008 *Phys. Plasmas* **15** 055704
- [55] Wigner E 1934 *Phys. Rev.* **46** 1002
- [56] Dubin D and O’Neil T 1999 *Rev. Mod. Phys.* **71** 87–172
- [57] Bonitz M, Filinov V S, Fortov V E, Levashov P R and Fehske H 2005 *Phys. Rev. Lett.* **95** 235006
- [58] Ikezi H 1986 *Phys. Fluids* **29** 1764–6
- [59] Farouki R T and Hamaguchi S 1992 *Appl. Phys. Lett.* **61** 2973–5
- [60] Verheest F 2000 *Waves in Dusty Space Plasmas* (Dordrecht: Kluwer)
- [61] Bouchoule A 1999 *Dusty Plasmas: Physics, Chemistry, and Technological Impacts in Plasma Processing* (New York: Wiley)
- [62] Hayashi Y and Tachibana K 1994 *Japan. J. Appl. Phys.* **33** L804–6
- [63] Melzer A, Trottenberg T and Piel A 1994 *Phys. Lett. A* **191** 301–8
- [64] Thomas H, Morfill G, Demmel V, Goree J, Feuerbacher B and Möhlmann D 1994 *Phys. Rev. Lett.* **73** 652–5
- [65] Bliokh P, Sinitin V and Yaroshenko V 1995 *Dusty and Self-gravitational Plasma in Space* (Dordrecht: Kluwer)
- [66] Morfill G E, Tsytovich V N and Thomas H 2007 *Elementary Physics of Complex Plasmas (Lecture Notes in Physics)* (Berlin: Springer)
- [67] Shukla P and Mamun M 2002 *Introduction to Dusty Plasma Physics* (Bristol: Institute of Physics Publishing)
- [68] Vladimirov S V, Ostrikov K and Samarian A A 2005 *Physics and Applications of Complex Plasmas* (London: Imperial College Press)
- [69] Morfill G E and Ivlev A V 2009 *Rev. Mod. Phys.* **81** 1353
- [70] Feng Y, Goree J and Liu B 2007 *Rev. Sci. Instrum.* **78** 053704
- [71] Ivanov Y and Melzer A 2007 *Rev. Sci. Instrum.* **78** 033506
- [72] Melzer A 2001 *Plasma Sources Sci. Technol.* **10** 303–10
- [73] Whipple E 1981 *Rep. Prog. Phys.* **44** 1197–250
- [74] Mott-Smith H and Langmuir I 1926 *Phys. Rev.* **28** 727–63
- [75] Whipple E, Northrop T and Mendis D 1985 *J. Geophys. Res.* **90** 7405–13
- [76] Miloch W, Pécseli H and Trulsen J 2007 *Nonlinear Process. Geophys.* **14** 575
- [77] Miloch W, Vladimirov S, Pécseli H and Trulsen J 2009 *New J. Phys.* **11** 043005
- [78] Barnes M, Keller J, Forster J, O’Neill J and Coultas D 1992 *Phys. Rev. Lett.* **68** 313–16
- [79] Hutchinson I 2005 *AIP Conf. Proc.* **799** 38–47
- [80] Lampe M 2001 *J. Plasma Phys.* **65** 171–80
- [81] Nitter T 1996 *Plasma Sources Sci. Technol.* **5** 93–111
- [82] Bryant P 2003 *J. Phys. D: Appl. Phys.* **36** 2859–68
- [83] Khrapak S et al 2005 *Phys. Rev. E* **72** 015406
- [84] Nairn C, Annaratone B and Allen J 1998 *Plasma Sources Sci. Technol.* **7** 478–90
- [85] Havnes O, Morfill G and Goertz C 1984 *J. Geophys. Res.* **89** 10999–11003
- [86] Yamaguchi H and Nejoh Y N 1999 *Phys. Plasmas* **6** 1048–51
- [87] Trottenberg T, Melzer A and Piel A 1995 *Plasma Sources Sci. Technol.* **4** 450–8
- [88] Homann A, Melzer A, Peters S, Madani R and Piel A 1997 *Phys. Rev. E* **56** 7138–41
- [89] Homann A, Melzer A, Peters S, Madani R and Piel A 1998 *Phys. Lett. A* **242** 173–80
- [90] Ratynskaia S, Kretschmer M, Khrapak S, Quinn R, Morfill G, Thoma M, Zobnin A, Usachev A, Petrov O and Fortov V 2004 *IEEE Trans. Plasma Sci.* **32** 613–616
- [91] Ratynskaia S et al 2004 *Phys. Rev. Lett.* **93** 085001
- [92] Konopka U, Ratke L and Thomas H 1997 *Phys. Rev. Lett.* **79** 1269–72
- [93] Ivlev A V, Morfill G E and Fortov V E 1999 *Phys. Plasmas* **6** 1415
- [94] Bronold F, Fehske H, Kersten H and Deutsch H 2008 *Phys. Rev. Lett.* **101** 175002
- [95] Trottenberg T, Brede B, Block D and Piel A 2003 *Phys. Plasmas* **10** 4627–32
- [96] Akdim M R 2003 *Modelling of complex plasmas PhD Thesis* Instituut voor Plasmafysica Rijnhuizen
- [97] Klindworth M, Piel A and Melzer A 2004 *Phys. Rev. Lett.* **93** 195002
- [98] Havnes O, Goertz C K, Morfill G E, Grün E and Ip W 1987 *J. Geophys. Res.* **92** 2281–7
- [99] Nitter T, Aslaksen T K, Melandsø F and Havnes O 1994 *IEEE Trans. Plasma Sci.* **22** 159–172
- [100] Cui C and Goree J 1994 *IEEE Trans. Plasma Sci.* **22** 151–158
- [101] Konopka U, Morfill G E and Ratke L 2000 *Phys. Rev. Lett.* **84** 891–894
- [102] Kompaneets R, Konopka U, Ivlev A V and Tsytovich V 2007 *Phys. Plasmas* **14** 052108
- [103] Melzer A, Schweigert V A and Piel A 1999 *Phys. Rev. Lett.* **83** 3194–3197
- [104] Melzer A, Schweigert V A and Piel A 2000 *Phys. Scr.* **61** 494–501
- [105] Melzer A, Schweigert V A, Schweigert I V, Homann A, Peters S and Piel A 1996 *Phys. Rev. E* **54** R46–9
- [106] Takahashi K, Oishi T, Shimomai K i, Hayashi Y and Nishino S 1998 *Phys. Rev. E* **58** 7805–11
- [107] Melandsø F and Goree J 1995 *Phys. Rev. E* **52** 5312–26
- [108] Melandsø F and Goree J 1996 *J. Vac. Sci. Technol. A* **14** 511–18
- [109] Nambu M, Vladimirov S and Shukla P 1995 *Phys. Lett. A* **203** 40–42
- [110] Schweigert V, Schweigert I, Melzer A, Homann A and Piel A 1996 *Phys. Rev. E* **54** 4155–66

- [111] Shukla P K and Rao N N 1996 *Phys. Plasmas* **3** 1770–72
- [112] Vladimirov S V and Ishihara O 1996 *Phys. Plasmas* **3** 444–6
- [113] Jellum G, Daugherty J and Graves D 1991 *J. Appl. Phys.* **69** 6923–34
- [114] Rothermel H, Hagl T, Morfill G, Thoma M and Thomas H 2002 *Phys. Rev. Lett.* **89** 175001
- [115] Talbot L, Cheng R K, Scheffer R W and Willis D R 1980 *J. Fluid Mech.* **101** 737–58
- [116] Arp O, Block D, Piel A and Melzer A 2004 *Phys. Rev. Lett.* **93** 165004
- [117] Carstensen J, Greiner F, Hou L J, Maurer H and Piel A 2009 *Phys. Plasmas* **16** 013702
- [118] Epstein P 1924 *Phys. Rev.* **23** 710–733
- [119] Hutchinson I 2005 *Plasma Phys. Control. Fusion* **47** 71–87
- [120] Hutchinson I 2006 *Plasma Phys. Control. Fusion* **48** 185–202
- [121] Khrapak S A, Ivlev A V, Morfill G E and Thomas H M 2002 *Phys. Rev. E* **66** 046414
- [122] Khrapak S, Ivlev A, Morfill G and Zhdanov S 2003 *Phys. Rev. Lett.* **90** 225002
- [123] Khrapak S, Ivlev A, Morfill G, Zhdanov S and Thomas H 2004 *IEEE Trans. Plasma Sci.* **32** 555–60
- [124] Khrapak S, Ivlev A, Zhdanov S and Morfill G 2005 *Phys. Plasmas* **12** 042308
- [125] Kilgore M, Daugherty J, Porteous R and Graves D 1993 *J. Appl. Phys.* **73** 7195–202
- [126] Khrapak S, Ivlev A, Morfill G, Thomas H, Zhdanov S, Konopka U, Thoma M and Quinn R 2003 *Phys. Plasmas* **10** 4579–81
- [127] Yaroshenko V et al 2005 *New Vistas in Dusty Plasmas AIP Conf. Proc.* **799** 239–42
- [128] Zafiu C, Melzer A and Piel A 2002 *Phys. Plasmas* **9** 4794
- [129] Zafiu C, Melzer A and Piel A 2003 *Phys. Plasmas* **10** 1278–82
- [130] Hirt M, Block D and Piel A 2004 *IEEE Trans. Plasma Sci.* **32** 582–5
- [131] Wolter M, Melzer A, Arp O, Klindworth M and Piel A 2007 *Phys. Plasmas* **14** 123707
- [132] Nosenko V, Fisher R, Merlino R, Khrapak S, Morfill G and Avinash K 2007 *Phys. Plasmas* **14** 103702
- [133] Liebermann M and Lichtenberg A 1994 *Principles of Plasma Discharges and Material processing* (New York: Wiley)
- [134] Pieper J and Goree J 1996 *Phys. Rev. Lett.* **77** 3137–40
- [135] Hayashi Y 1999 *Phys. Rev. Lett.* **83** 4764–7
- [136] Pieper J, Goree J and Quinn R 1996 *Phys. Rev. E* **54** 5636–40
- [137] Zuzic M, Ivlev A, Goree J, Morfill G, Thomas H, Rothermel H, Konopka U, Sütterlin R and Goldbeck D 2000 *Phys. Rev. Lett.* **85** 4064–7
- [138] Zobnin A, Nefedov A, Sinel'shchikov V, Sinkevich O, Usachev A, Filippov V and Fortov V 2000 *Plasma Phys. Rep.* **26** 415–23
- [139] Goree J, Morfill G, Tsyтович V and Vladimirov S 1999 *Phys. Rev. E* **59** 7055–67
- [140] Morfill G, Thomas H, Konopka U, Rothermel H, Zuzic M, Ivlev A and Goree J 1999 *Phys. Rev. Lett.* **83** 1598–601
- [141] Barkan A and Merlino R 1995 *Phys. Plasmas* **2** 3261
- [142] Thompson C, Barkan A, D'Angelo N and Merlino R L 1997 *Phys. Plasmas* **4** 2331–5
- [143] Trottenberg T, Block D and Piel A 2006 *Phys. Plasmas* **13** 042105
- [144] Pilch I, Reichstein T and Piel A 2008 *Phys. Plasmas* **15** 103706
- [145] Barkan A, Merlino R and D'Angelo N 1995 *Phys. Plasmas* **2** 3563–5
- [146] Pilch I, Piel A, Trottenberg T and Koepke M E 2007 *Phys. Plasmas* **14** 123704
- [147] Nefedov A P et al 2003 *New J. Phys.* **5** 33
- [148] Annaratone B M, Glier M, Stuffer T, Raif M, Thomas H M and Morfill G E 2003 *New J. Phys.* **5** 92
- [149] Bryant P 2004 *New J. Phys.* **6** 1–15
- [150] Ivlev A, Thomas H, Morfill G, Molotkov V, Lipaev A, Fortov V, Hagl T, Rothermel H and Krialev S 2006 *New J. Phys.* **8** 25
- [151] Fortov V E, Vaulina O S, Petrov O F, Molotkov V I, Lipaev A M, Morfill G E, Thomas H, Khrapak S A, Semenov Y P and Ivanov A I 2004 *Plasma Phys. Control. Fusion* **46** B359–366
- [152] Fortov V E et al 2003 *Phys. Rev. Lett.* **90** 245005
- [153] Khrapak S et al 2003 *Phys. Plasmas* **10** 1–4
- [154] Piel A, Klindworth M, Arp O, Melzer A and Wolter M 2006 *Phys. Rev. Lett.* **97** 205009
- [155] Samsonov D, Morfill G, Thomas H, Hagl T and Rothermel H 2003 *Phys. Rev. E* **67** 036404
- [156] Yaroshenko V et al 2004 *Phys. Rev. E* **69** 066401
- [157] Tsyтович V, Vladimirov S, Morfill G and Goree J 2001 *Phys. Rev. E* **63** 056609
- [158] Tsyтович V, Vladimirov S, Morfill G and Goree J 2001 *Phys. Rev. E* **64** 029902
- [159] Tsyтович V 2001 *Phys. Scr.* **89** 89–94
- [160] Akdim M R and Goedheer W J 2002 *Phys. Rev. E* **65** 015401
- [161] Land V, Goedheer W and Akdim M 2005 *Phys. Rev. E* **72** 046403
- [162] Land V and Goedheer W 2006 *New J. Phys.* **8** 8
- [163] Praburam G and Goree J 1996 *Astrophys. J.* **441** 830–8
- [164] Lipaev A M et al 2007 *Phys. Rev. Lett.* **98** 265006
- [165] Rao N, Shukla P and Yu M 1990 *Planet. Space Sci.* **38** 543–6
- [166] D'Angelo N 1990 *Planet. Space Sci.* **38** 1143–6
- [167] Shukla P and Silin V 1992 *Phys. Scr.* **45** 508
- [168] Melandsø F 1996 *Phys. Plasmas* **3** 3890–901
- [169] Peeters F and Wu X 1987 *Phys. Rev. A* **35** 3109–14
- [170] Luo Q, D'Angelo N and Merlino R 1999 *Phys. Plasmas* **6** 3455–8
- [171] Nakamura Y, Bailung H and Shukla P 1999 *Phys. Rev. Lett.* **83** 1602–5
- [172] Samsonov D, Zhdanov S K, Quinn R A, Popel S I and Morfill G E 2004 *Phys. Rev. Lett.* **92** 255004
- [173] Dubin D 2000 *Phys. Plasmas* **7** 3895–903
- [174] Havnes O, Aslaksen T, Hartquist T, Li F, Melandsø F, Morfill G and Nitter T 1995 *J. Geophys. Res.* **100** 1731–4
- [175] Melzer A, Nunomura S, Samsonov D and Goree J 2000 *Phys. Rev. E* **62** 4162–76
- [176] Samsonov D, Goree J, Ma Z, Bhattacharjee A, Thomas H and Morfill G 1999 *Phys. Rev. Lett.* **83** 3649–52
- [177] Misawa T, Ohno N, Asano K, Sawai M, Takamura S and Kaw P 2001 *Phys. Rev. Lett.* **86** 1219–22
- [178] Piel A, Nosenko V and Goree J 2006 *Phys. Plasmas* **13** 042104
- [179] Vladimirov S, Shevchenko P and Cramer N 1997 *Phys. Rev. E* **56** R74–6
- [180] Wang X, Bhattacharjee A and Hu S 2001 *Phys. Rev. Lett.* **86** 2569–72
- [181] Shukla P K and Eliasson B 2009 *Rev. Mod. Phys.* **81** 25
- [182] Melzer A, Homann A and Piel A 1996 *Phys. Rev. E* **53** 2757–66
- [183] Schweigert V, Schweigert I, Melzer A, Homann A and Piel A 1998 *Phys. Rev. Lett.* **80** 5345
- [184] Schweigert I, Schweigert V, Melzer A and Piel A 2000 *JETP Lett.* **71** 58–61
- [185] Thomas H and Morfill G 1996 *Nature* **379** 806–9
- [186] Nosenko V, Zhdanov S K, Ivlev A V, Knapek C A and Morfill G E 2009 *Phys. Rev. Lett.* **103** 015001
- [187] Juan W T and I L 1998 *Phys. Rev. Lett.* **80** 3073
- [188] Liu B, Goree J and Vaulina O S 2006 *Phys. Rev. Lett.* **96** 015005
- [189] Liu B and Goree J 2007 *Phys. Rev. E* **75** 016405
- [190] Nunomura S, Samsonov D, Zhdanov S and Morfill G 2006 *Phys. Rev. Lett.* **96** 015003

- [191] Ratynskaia S, Rypdal K, Knapek C, Khrapak S, Milovanov A V, Ivlev A, Rasmussen J J and Morfill G E 2006 *Phys. Rev. Lett.* **96** 105010
- [192] Vaulina O S and Vladimirov S V 2002 *Phys. Plasmas* **9** 835
- [193] Mortensen A, Nielsen E, Matthey T and Drewsen M 2006 *Phys. Rev. Lett.* **96** 103001
- [194] Totsuji H, Kishimoto T, Totsuji C and Tsuruta K 2002 *Phys. Rev. Lett.* **88** 125002
- [195] Itano W M, Bollinger J J, Tan J N, Jelenkovic B, Huang X P and Wineland D J 1998 *Science* **279** 686–9
- [196] Thomson J J 1904 *Phil. Mag.* **39** 237–65
- [197] Paul W 1990 *Rev. Mod. Phys.* **62** 531–40
- [198] Diederich F, Peik E, Chen J M, Quint W and Walther H 1987 *Phys. Rev. Lett.* **59** 2931–4
- [199] Gilbert S L, Bollinger J J and Wineland D J 1988 *Phys. Rev. Lett.* **60** 2022–5
- [200] Bollinger J, Mitchell T, Huang X, Itano W, Tan J, Jelenkovic B and Wineland D 2000 *Phys. Plasmas* **7** 7
- [201] Hasse R W and Avilov V V 1991 *Phys. Rev. A* **44** 4506–15
- [202] Tsuruta K and Ichimaru S 1993 *Phys. Rev. A* **48** 1339
- [203] Mackay A L 1962 *Acta Crystallogr.* **15** 916–18
- [204] Baletto F and Ferrando R 2005 *Rev. Mod. Phys.* **77** 371–423
- [205] Kjaergaard N and Drewsen M 2003 *Phys. Rev. Lett.* **91** 095002
- [206] Hornekaer L, Kjaergaard N, Thommesen A M and Drewsen M 2001 *Phys. Rev. Lett.* **86** 1994–7
- [207] Matthey T, Hansen J P and Drewsen M 2003 *Phys. Rev. Lett.* **91** 165001
- [208] Juan W T, Huang Z H, Hsu J W, Lai Y J and I L 1998 *Phys. Rev. E* **58** R6947–50
- [209] Klindworth M, Melzer A, Piel A and Schweigert V 2000 *Phys. Rev. B* **61** 8404–10
- [210] Melzer A, Klindworth M and Piel A 2001 *Phys. Rev. Lett.* **87** 115002
- [211] Miksch T and Melzer A 2007 *Phys. Rev. E* **75** 016404
- [212] Bedanov V and Peeters F 1994 *Phys. Rev. B* **49** 2667–76
- [213] Schweigert V and Peeters F 1995 *Phys. Rev. B* **51** 7700
- [214] Annaratone B M, Antonova T, Goldbeck D D, Thomas H M and Morfill G E 2004 *Plasma Phys. Control. Fusion* **46** B495–509
- [215] Antonova T, Annaratone B, Goldbeck D, Yaroshenko V, Thomas H and Morfill G 2006 *Phys. Rev. Lett.* **96** 115001
- [216] Block D, Kroll M, Arp O, Piel A, Käding S, Ivanov Y, Melzer A, Baumgartner H, Henning C and Bonitz M 2007 *Plasma Phys. Control. Fusion* **49** B109–16
- [217] Goedheer W, Land V and Venema J 2009 *Contrib. Plasma Phys.* **49** 199
- [218] Lampe M, Joyce G, Ganguli G and Gavrishchaka V 2000 *Phys. Plasmas* **7** 10
- [219] Joyce G, Lampe M and Ganguli G 2002 *Phys. Rev. Lett.* **88** 095006
- [220] Bonitz M, Block D, Arp O, Golubnychiy V, Baumgartner H, Ludwig P, Piel A and Filinov A 2006 *Phys. Rev. Lett.* **96** 075001
- [221] Ludwig P, Kosse S and Bonitz M 2005 *Phys. Rev. E* **71** 046403
- [222] Arp O, Block D, Bonitz M, Fehske H, Golubnychiy V, Kosse S, Ludwig P, Melzer A and Piel A 2005 *J. Phys.: Conf. Ser.* **11** 234–47
- [223] Block D, Arp O, Piel A and Melzer A 2005 *New Vistas in Dusty Plasmas AIP Conf. Proc.* **799** 454
- [224] Baumgartner H, Asmus D, Golubnychiy V, Ludwig P, Kählert H and Bonitz M 2008 *New J. Phys.* **10** 093019
- [225] Kraeft W D and Bonitz M 2006 *J. Phys.: Conf. Ser.* **35** 94–109
- [226] Henning C, Baumgartner H, Piel A, Ludwig P, Golubnychiy V, Bonitz M and Block D 2006 *Phys. Rev. E* **74** 056403
- [227] Cioslowski J and Grzebielucha E 2008 *Phys. Rev. E* **78** 026416
- [228] Cioslowski J 2008 *J. Chem. Phys.* **128** 164713
- [229] Totsuji H, Ogawa T, Totsuji C and Tsuruta K 2005 *Phys. Rev. E* **72** 036406
- [230] Baumgartner H, Kählert H, Golubnychiy V, Henning C, Käding S, Melzer A and Bonitz M 2007 *Contrib. Plasma Phys.* **47** 281–90
- [231] Henning C, Ludwig P, Filinov A, Piel A and Bonitz M 2007 *Phys. Rev. E* **76** 036404
- [232] Wrighton J W, Dufty C H and Bonitz M 2009 *J. Phys. A: Math. Gen.* **42** 214052
- [233] Block D, Käding S, Melzer A, Piel A, Baumgartner H and Bonitz M 2008 *Phys. Plasmas* **15** 040701
- [234] Käding S, Block D, Melzer A, Piel A, Kählert H, Ludwig P and Bonitz M 2008 *Phys. Plasmas* **15** 073710
- [235] Apolinario S W S and Peeters F M 2007 *Phys. Rev. E* **76** 031107
- [236] Dubin D H E 1996 *Phys. Rev. E* **53** 5268
- [237] Dubin D H E and Schiffer J P 1996 *Phys. Rev. E* **53** 5249
- [238] Calvo F and Yurtsever E 2007 *Eur. Phys. J. D* **44** 81–91
- [239] Sheridan T E 2005 *Phys. Rev. E* **72** 026405
- [240] Amiranashvili S G, Gusein-Zade N G and Tsyтович V N 2001 *Phys. Rev. E* **64** 016407
- [241] Dykeman E C and Sankey O F 2008 *Phys. Rev. Lett.* **100** 028101
- [242] van Vlijmen H and Karplus M 1993 *J. Chem. Phys.* **115** 8747
- [243] Posada-Amarillas A and Garzon I 1996 *Phys. Rev. B* **54** 11796
- [244] Wales D 1991 *J. Chem. Soc. Faraday Trans.* **87** 2399–405
- [245] Kählert H, Ludwig P, Baumgartner H, Bonitz M, Block D, Käding S, Melzer A and Piel A 2008 *Phys. Rev. E* **78** 036408
- [246] Kohn W 1961 *Phys. Rev.* **123** 1242
- [247] Brey L, Johnson N and Halperin B 1989 *Phys. Rev. B* **40** 10647
- [248] Henning C, Kählert H, Ludwig P, Melzer A and Bonitz M 2009 *J. Phys. A: Math. Gen.* **42** 214023
- [249] Sheridan T E 2006 *J. Phys. D: Appl. Phys.* **39** 693–9
- [250] Sheridan T E 2006 *Phys. Plasmas* **13** 022106
- [251] Stringari S 1996 *Phys. Rev. Lett.* **77** 2360
- [252] Guery-Odelin D, Zambelli F, Dalibard J and Stringari S 1999 *Phys. Rev. A* **60** 4851
- [253] Kinast J, Turlapov A and Thomas J E 2004 *Phys. Rev. A* **70** 051401
- [254] Bauch S, Balzer K, Henning C and Bonitz M 2009 *Phys. Rev. B* **80** 054515
- [255] Moritz H, Stöferle T, Köhl M and Esslinger T 2003 *Phys. Rev. Lett.* **91** 250402
- [256] Partoens B, Schweigert V A and Peeters F M 1997 *Phys. Rev. Lett.* **79** 3990
- [257] Kong M, Partoens B and Peeters F M 2003 *New J. Phys.* **5** 23
- [258] Sheridan T E 2005 *Phys. Plasmas* **12** 080701
- [259] Fortov V E, Ivlev A V, Khrapak S A, Khrapak A G and Morfill G E 2005 *Phys. Rep.* **421** 1–103
- [260] Olivetti A, Barré J, Marcos B, Bouchet F and Kaiser R 2009 *Phys. Rev. Lett.* **103** 224301
- [261] Henning C, Fujioka K, Ludwig P, Piel A, Melzer A and Bonitz M 2008 *Phys. Rev. Lett.* **101** 045002
- [262] Melzer A 2003 *Phys. Rev. E* **67** 016411
- [263] Piel A and Melzer A 2002 *Plasma Phys. Control. Fusion* **44** R1–R26
- [264] Melzer A, Block D and Piel A 2007 *Phys. J.* **6** 31
- [265] Ivanov Y and Melzer A 2009 *Phys. Rev. E* **79** 036402
- [266] Kählert H 2008 First principle simulations of classical charged particles in traps *Diploma Thesis* Kiel University
- [267] Balzer K, Nölle C, Bonitz M and Filinov A 2006 *J. Phys.: Conf. Ser.* **35** 209–18

- [268] Balzer K, Nölle C, Bonitz M and Filinov A 2006 *Phys. Status Solidi c* **3** 2402–5
- [269] Bonitz M, Balzer K and van Leeuwen R 2007 *Phys. Rev. B* **76** 045341
- [270] Geller M and Vignale G 1996 *Phys. Rev. B* **53** 6979
- [271] Pedri P, Palo S D, Orignac E, Citro R and Chiofalo M 2008 *Phys. Rev. A* **77** 015601
- [272] Hartmann P, Donkó Z, Bakshi P M, Kalman G J and Kyrkos S 2007 *IEEE Trans. Plasma Sci.* **35** 332–6
- [273] Böning J, Filinov A, Ludwig P, Baumgartner H, Bonitz M and Lozovik Y E 2008 *Phys. Rev. Lett.* **100** 113401
- [274] Lindemann F 1910 *Phys. Z.* **11** 609
- [275] Landau L and Lifshitz E 1969 *Statistical Physics* (Reading, MA: Addison-Wesley)
- [276] Mermin N 1968 *Phys. Rev.* **176** 250
- [277] Bedanov V, Gadiyak G and Lozovik Y 1985 *Phys. Lett. A* **109** 289–91
- [278] Eters R and Kaelberer J 1975 *Phys. Rev. A* **11** 1068
- [279] Berry R 1988 *Adv. Chem. Phys.* **B 70** 75
- [280] Löwen H 1994 *Phys. Rep.* **237** 249
- [281] Kosterlitz J and Thouless D 1973 *J. Phys. C: Solid State Phys. C* **6** 1181
- [282] Halperin B and Nelson D 1973 *Phys. Rev. Lett.* **41** 121
- [283] Knapek C, Samsonov D, Zhdanov S, Konopka U and Morfill G 2007 *Phys. Rev. Lett.* **98** 015004
- [284] Filinov A, Bonitz M and Lozovik Y 2001 *Phys. Rev. Lett.* **86** 3851
- [285] Filinov A, Lozovik Y and Bonitz M 2000 *Phys. Status Solidi b* **221** 231
- [286] Piacente G, Schweigert I V, Betouras J J and Peeters F M 2004 *Phys. Rev. B* **69** 045324
- [287] Apolinario S W S, Partoens B and Peeters F M 2006 *Phys. Rev. E* **74** 031107
- [288] Baumgartner H, Block D and Bonitz M 2009 *Contrib. Plasma Phys.* **49** 281–302
- [289] Golubnychiy V, Baumgartner H, Bonitz M, Filinov A and Fehske H 2006 *J. Phys. A: Math. Gen.* **39** 4527–31
- [290] Schiffer J 2002 *Phys. Rev. Lett.* **88** 205003
- [291] Alder B and Wainwright T 1970 *Phys. Rev. A* **1** 18
- [292] Juan W T, Chen M H and I L 2001 *Phys. Rev. E* **64** 016402
- [293] Lai Y J and I L 2002 *Phys. Rev. Lett.* **89** 155002
- [294] Quinn R and Goree J 2002 *Phys. Rev. Lett.* **88** 195001
- [295] Ratynskaia S, Knapek C, Rypdal K, Khrapak S and Morfill G E 2005 *Phys. Plasmas* **12** 022302
- [296] Liu B and Goree J 2008 *Phys. Rev. Lett.* **100** 055003
- [297] Liu B and Goree J 2008 *Phys. Rev. E* **78** 046403
- [298] Chan C and I L 2009 *Contrib. Plasma Phys.* **49** 215
- [299] Vaulina O S and Dranzhevski I E 2006 *Phys. Scr.* **73** 577
- [300] Hou L J, Piel A and Shukla P 2009 *Phys. Rev. Lett.* **102** 085002
- [301] Ott T, Bonitz M and Hartmann P 2009 *Phys. Rev. Lett.* **103** 099501
- [302] Donko Z, Goree J and Hartmann P 2009 *Phys. Rev. E* **79** 026401
- [303] Ott T, Bonitz M, Donkó Z and Hartmann P 2008 *Phys. Rev. E* **78** 026409
- [304] Donkó Z, Kalman G J and Golden K I 2002 *Phys. Rev. Lett.* **88** 225001
- [305] Donkó Z, Hartmann P and Kalman G J 2003 *Phys. Plasmas* **10** 1563–8
- [306] Ott T and Bonitz M 2009 *Phys. Rev. Lett.* **103** 195001
- [307] Ott T and Bonitz M 2009 *Contrib. Plasma Phys.* **49** 760
- [308] Kraeft W D and Bonitz M 2006 *J. Phys.: Conf. Ser.* **35** 78–93
- [309] Wrighton J, Dufty J, Kählert H and Bonitz M 2009 *Phys. Rev. E* **80** 066405
- [310] Wrighton J, Dufty J, Bonitz M and Kählert H 2010 *Contrib. Plasma Phys.* **80** 26–30
- [311] Evans R 1992 *Fundamentals of Inhomogeneous Fluids* (New York: Dekker)
- [312] Ng K 1974 *J. Chem. Phys.* **61** 2680–9
- [313] Kalman G and Golden K I 1990 *Phys. Rev. A* **41** 5516–27
- [314] Golden K I, Kalman G and Wyns P 1992 *Phys. Rev. A* **46** 3454–62
- [315] Rosenberg M and Kalman G 1997 *Phys. Rev. E* **56** 7166–7 173
- [316] Ivlev A V et al 2008 *Phys. Rev. Lett.* **100** 095003
- [317] Ludwig P, Filinov A, Bonitz M and Stolz H 2006 *Phys. Status solidi b* **243** 2363
- [318] Kählert H and Bonitz M 2010 *Phys. Rev. Lett.* **104** 015001
- [319] Kählert H and Bonitz M 2010 *Contrib. Plasma Phys.* at press, doi:10.1002/ctpp.201010105
- [320] Ivlev A, Steinberg V, Kompaneets R, Höfner H, Sidorenko I and Morfill G E 2007 *Phys. Rev. Lett.* **98** 145004